COMPUTATIONAL STUDIES OF CAMBRIDGE STRATIFIED PREMIXED FLAMES USING TRANSPORTED PROBABILITY DENSITY FUNCTION METHOD

by

Krutika Appaswamy

A Thesis

Submitted to the Faculty of Purdue University

In Partial Fulfillment of the Requirements for the degree of

Master of Science

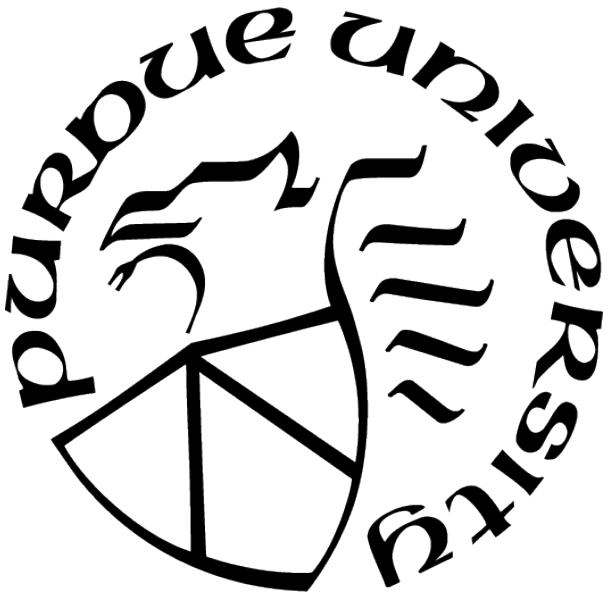

School of Aeronautics and Astronautics

West Lafayette, Indiana

August 2021

THE PURDUE UNIVERSITY GRADUATE SCHOOL
STATEMENT OF COMMITTEE APPROVAL

Dr. Haifeng Wang, Chair

School of Aeronautics and Astronautics

Dr. Li Qiao

School of Aeronautics and Astronautics

Dr. Tom Shih

School of Aeronautics and Astronautics

Approved by:

Dr. Gregory Blaisdell

ACKNOWLEDGMENTS

Firstly, I would like to express my highest gratitude to my advisor, Dr.Haifeng Wang, for giving me the opportunity to work with him on this project. His guidance, support and persistent patience to teach has led me throughout the course of this study. I would also like to thank Dr. Li Qiao and Dr. Tom Shih for taking the time to be on my committee and offer their guidance.

I would also like profusely thank all the members of the Computational Energy and Propulsion Laboratory at Purdue University, Dr. Xinran Zhao, Dr. Jinlong Liu, Tianfang Xie, Utsav Jain, Jei Tao, Abhinand Ayyaswamy and Biswaranjan Pati for their prompt help and support.

All the computational simulations would not have been possible without the computational resources provided by the Research Computing Center and Engineering Computer Network (ECN) as well as support by Information Technology at Purdue (ITaP) at Purdue University .

I could not have been in this position without the constant support and encouragement from my parents, Mr.and Mrs. Appaswamy , who have made sure I get every support and resource possible to follow my aspirations.

Purdue University's Engineering Computer Network and Graduate School helped fund PurdueThesis development.

TABLE OF CONTENTS

LIST OF TABLES

LIST OF FIGURES

ABSTRACT

Computational studies are performed on a Cambridge Stratified Swirl burner (SwB), a lean premixed stratified flame, by using the Reynolds Averaged Navier Stokes (RANS) model and the transported Probability Density Function (PDF) model. The SwB burner was measured by Sweeney et al. (Combustion and Flame, 2012, 159: 2896-2911), and comprehensive data are available for model validation, e.g., the mean and root-mean-square values of velocity, temperature, and species mass fractions. The experimental data are available for sixteen different cases to investigate flames in premixed and stratified regimes, with or without swirl. In this study, we consider only non-swirling, premixed and stratified cases. Different turbulence models are examined in the modeling studies, and the Reynolds Stress model with standard model constant values is found to perform well with the transported PDF model. A joint PDF for enthalpy and species mass fractions allows for the highly non-linear reaction term in the transport equation to be completely closed. The mixing term arising from molecular diffusion is not closed and requires modeling which is a significant challenge. For the SwB, we consider a series of mixing models including the Interaction by Exchange with the Mean (IEM) mixing model with different mixing model constants, the Modified Curl model, and two mixing models designed for premixed combustion from the literature. We first examine the models in the non-stratified/premixed case (SwB1) to isolate the effect of other conditions from stratification on the model predictions. The stratification is then added in two levels, a moderately stratified case (SwB5) and a highly stratified case (SwB9). The predicted results are compared with the experimental data at various locations, inside and outside the recirculation zone in the burner. In general, good agreement is obtained for the velocity fields inside the recirculation zone. Good agreement is also obtained of the predicted and measured results is obtained for the mean values of temperature and species mass fractions. The scalar fluctuations are generally underpredicted. Overall, the employed modeling method is able to capture the mean flame structure reasonably well in lean premixed stratified flames. Some limitations are noticed, e.g., the underprediction of scalar fluctuations, and overprediction of CH_4 concentration in the stratified cases. These observations are useful for guiding the future research directions.

1. INTRODUCTION

1.1 Importance of combustion research

For centuries, combustion or burning of fossil fuels has been one of mankind's primary sources of energy in the form of heat. This released energy can be converted to many forms such as electricity and thrust. Since their advent, all engines, including rockets, worked with some form of combustion of fuel. Until 2012, 81 percent of energy consumed in U.S. was from petroleum, natural gas and coal [1]. While this number has slightly reduced due to growing attempts at using renewable forms of energy, as shown in Figure 1.1, combustion of fossil fuels is still the major source of energy for most industrial, transport, and electricity generating applications. Incineration is also a common method of waste disposal.

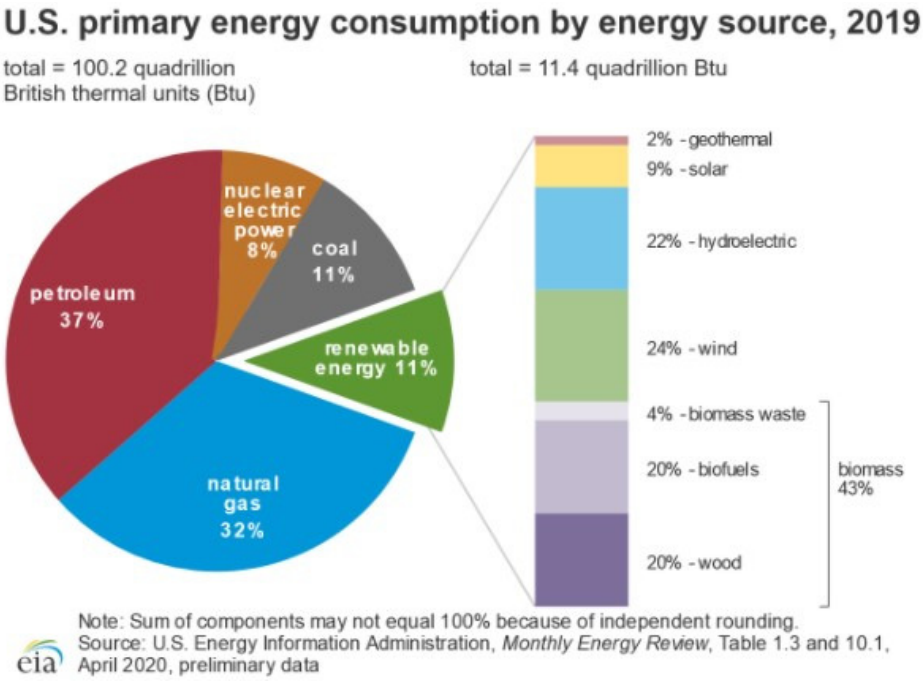

Figure 1.1. The figure shows the energy sources and their respective percentages for the energy consumption in the United States. (Image taken from [2].)

While the importance of combustion is evident, there are still significant issues with leaning on conventional fuel combustion, such as air pollution and the rapid depletion of fossil fuels due to increasing energy demands. Furthermore, combustion of fossil fuels results

in by-products such as unburned or partially burned hydrocarbons, nitrogen oxides (NO and NO_2), carbon monoxides, sulfur oxides (SO_2 and SO_3), and particulate matter in various forms [3]. One of the common by-products, carbon dioxide, is a greenhouse gas and is the most significant contributor to the increasing global warming. In addition, nitrogen oxides contribute to the depletion of the ozone layer, while sulfur oxides play an important role in acid rain. Hence, adequate research and knowledge are required to obtain maximum energy from combustion while reducing pollutant production.

1.2 Types of flames

Different types of flames can result from how the fuel and oxidant are mixed in a burner and their flow rates. Premixed gas flames can arise from fuel gas and air being mixed prior to entering the burner, as shown in Figure 1.2a, where the premix of gas and air enters the Bunsen burner. As shown in Figure 1.2b, if they mix after leaving the burner (like in a candle), they are called diffusion flames. The gas flow rate may be relatively low, in which case, the incoming gaseous flow of fuel and air is laminar, as is the flame. With high gas flows, they may be turbulent. Thus, flames can be laminar premixed, laminar diffusion, turbulent premixed, or turbulent diffusion flames [4]. In this study, we are going to be looking at a turbulent premixed stratified flame. In the past two decades, lean premixed combustion has become the leading technology for controlling NO_x emissions [5] and hence has great potential for environmental benefits.

1.3 Stratified Combustion

As stated earlier, lean premixed flames (especially low-temperature combustion) are a promising solution for reducing NO_x emissions in gas turbines. Due to the short mixing time, the mixture may not be homogeneous and may have patches of rich or stoichiometric regions. So, locally lean, rich, and stoichiometric regions can be observed in different parts of the combustion chamber at the same time. The term stratified burning may include both this in-homogeneous premixed combustion and the mixing controlled after burning of lean and rich products [8]. Stratification can also offer some flame stability to overall lean

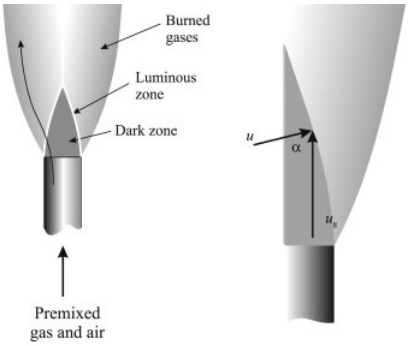

(a) A Bunsen burner is a good example of a premixed flame where the fuel and oxidiser are mixed before combustion takes place. (Image taken from [6].)

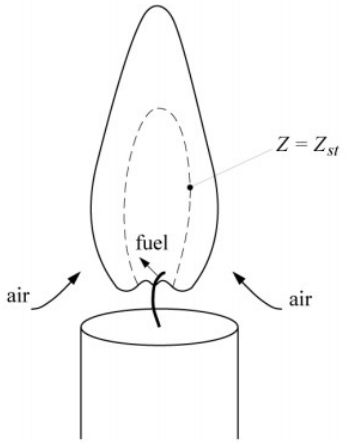

(b) A candle is an example of a non premixed flame where the fuel and the oxidiser (air) separately enter the combustion zone. (Image taken from [7].)

Figure 1.2. Schematic diagram of examples of premixed and non-premixed combustion.

combustion as shown by the factors in Figure 1.3, which is why we are interested in the study of premixed lean stratified flames. The high efficiency of stratified lean combustion is attributable to two factors, dethrottling and improvement of combustion efficiency [9]. Investigations on stratified flames have focused mainly on coflowing configurations to allow for easier modeling of the data. In contrast, more complex bluff-body flames have received less extensive investigation [10]. The current computational study is of the Cambridge Stratified burner [11], a lean stratified swirl burner. We focus only on the non-swirling cases to isolate the effects of stratification without the additional difficulty of dealing with swirling flows.

1.4 Focus of this study

The current study is the computational study of the Cambridge Stratified Flame using the transported probability density function (PDF) method [12]. Ansys FLUENT [13] is used as the tool for the computational studies as it is a robust software, and the parameters of the case were found within the tool's scope. Lean premixed combustion has been widely adopted in practical combustion systems for it can offer low NO_x emission by decreasing peak reacting

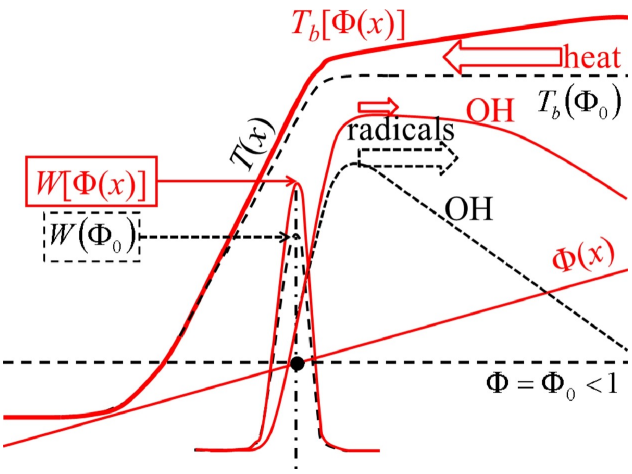

Figure 1.3. Comparison of flame properties of Homogeneously premixed (dashed lines) and back-supported stratified (solid lines) laminar flames. (Image taken from [8].)

temperature. In practical cases, such combustion takes place under stratified combustion to aid with the mixing. However, a complete understanding of stratified combustion is still out of reach, and to this end, the Cambridge Stratified Swirl Combustor (SwB) [11] was created. While stratified flames have been studied extensively, lean premixed stratified flames still require some investigation. The Cambridge burner, the Darmstadt burner [14], and the V-shaped flames [15] are a few burners that aid this investigation.

Since stratified flames lie between premixed flames and non-premixed flames, current premixed/non-premixed combustion models cannot be directly applied; hence, the PDF method was used. The PDF method can directly solve the transport equation and hence, in theory, can directly solve stratified cases without special modifications. This is shown in the results. The Cambridge burner was designed to have an open flame, facilitating high fidelity scalar measurements [11]. These design decisions were also made in the context of providing model test cases progressively more complex and therefore complementary to those of the Darmstadt stratified burner [14]. The present burner is similar in that it uses a co-annular design but imposes additional flow complexity by including a bluff-body induced recirculation zone [11]. Figure 1.4 shows the Cambridge burner flames at different swirl and stratification levels.

In literature, various numerical models have been proposed for stratified turbulent combustion. Previous computational studies on the Cambridge burner usually employ high-cost, high fidelity, Large Eddy Simulation (LES) methods with various sub-grid scale and combustion models. Brauner et al. [16] utilized the sub-grid scale PDF approach, which was rearranged so that the resolved and sgs components are separated. While the predicted mean and RMS values were in good agreement with the experimental values near the bluff body, discrepancies were observed further downstream. Proch et al. [17] used the artificially thickened flame LES combined with tabulated premixed flame chemistry. Mercier et al. [18] used flame surface density (FSD) and Filtered Tabulated Chemistry for LES (F-TACLES) but have similar RMS value agreement as Braunner et al. [16]. Other LES studies include Zhang et al. [19] using dynamic thickened flame (DTF) with flamelet generated manifolds (FGM) tabulation approach and Xiao et al. [20] who used finite rate chemistry to model combustion. More recently, Turkeri et al. [21] performed LES/probability density function calculations and obtained good agreement with the experimental. This year, Zhang et al. [22] used LES and FGM combustion model to look at the effects of non-unity Lewis number.

As it can be seen, premixed stratified flames are still an important subject to be studied, and there are plenty of methods and models to study it computationally. Previous studies have focused mainly on LES, which can be computationally very expensive. The mixing model is critical because combustion occurs at the smallest molecular scales when reactants and heat diffuse together. Modeling mixing in PDF method is not straightforward and is the weakest link in the PDF method. A few different mixing models are implemented, and the effects are observed. This study aims to obtain accurate predictions while significantly reducing computational costs. This work focuses on only the non-swirling flame cases of the burner experiments. A two-dimensional asymmetric domain is chosen, and we aim to model the turbulent recirculation zone that formed due to the bluff body which stabilizes the flame. Hence, higher emphasis is placed on the region within the recirculation zone. Effects of different turbulence models, combustion models, and boundary conditions are also noted.

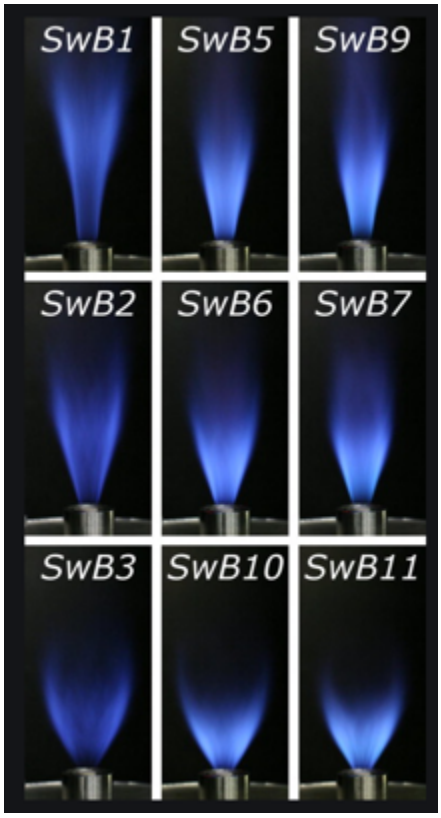

Figure 1.4. Cambridge Stratified Burner Flames. Each column is a different level of stratification while each row shows a different level of swirl. (Image taken from [23].)

1.5 Major Contributions

This work focuses on the two-dimensional Reynolds Averaged Navier Stokes (RANS) modeling of the Cambridge burner to identify models that capture the prominent features of the flame accurately. For this purpose, obtained simulation results are compared with the experimental values. The following are claimed as major contributions of this study:

1) Verifying the benefits of using the transported PDF method on stratified combustion for two-dimensional axisymmetric cases. This helps showing the effectiveness of the model beyond three-dimensional LES simulations.

2) Implementing different mixing models and comparing their ability to capture mixing in the presence of stratification.

3) Improving the results obtained by the transported PDF method with the help of these

mixing models.

4) Comparing the performance of different turbulence models to capture the recirculation zone.

With the knowledge gained from this study, we can now identify the benefits and the drawbacks of using two-dimensional modeling of stratified turbulent combustion. We can now identify what factors dominate the flow in different regions. This study lays the groundwork for more research into mixing in stratified flames.

2. CAMBRIDGE STRATIFIED SWIRL BURNER

This chapter gives a detailed description of the Cambridge Stratified Swirl burner (SwB). The operating conditions of the burner will also be discussed, along with modeling challenges and strategies. The flame characteristics, as well as the experimental results, will be discussed.

2.1 Burner description

A Stratified Swirl burner was essentially used as an improvement to the slot burner as it has higher flow rates, velocities, and turbulence. Swirl rates and stratification ratios are varied to generate various experimental conditions to allow the investigation of their separate and combined effects [11].

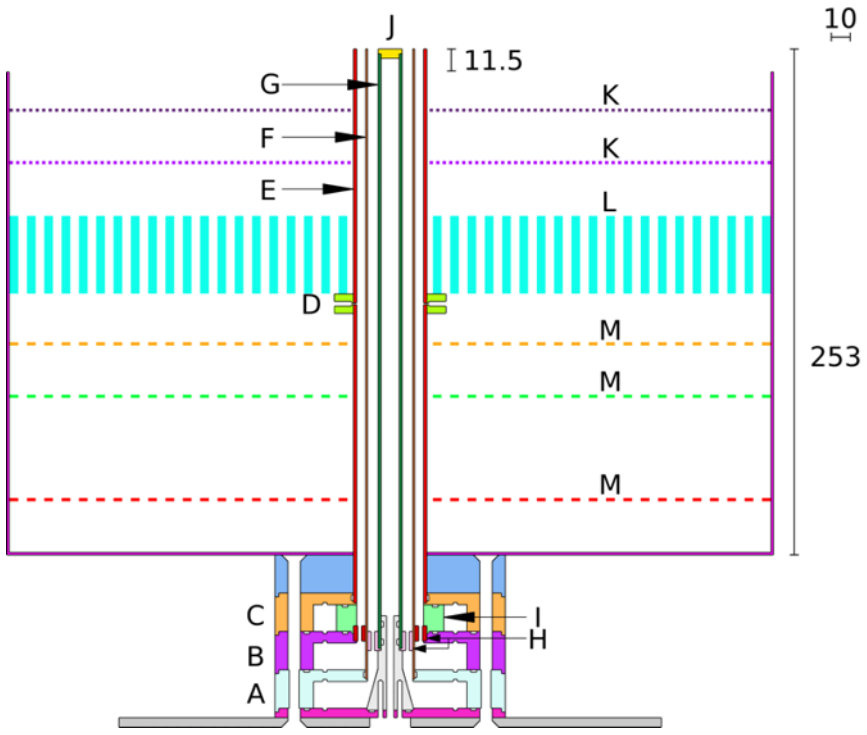

Figure 2.1. Elevation of the stratified swirl burner. A: inner annulus plenum; B: outer annulus axial flow plenum; C: outer annulus swirl flow plenum; D: locating collar; E: outer tube; F: middle tube; G: inner tube; H: flow straighteners; I: swirl generating collar; J: ceramic cap; K: wire mesh; L: honeycomb section; M: perforated disk. Flow fittings are omitted for clarity. (Image taken from [11].)

Figure 2.1 shows the sectional front view of the burner. It has two annular pipes through which the methane/air premix flows (they may have different fuel/air ratios) and a large coflow region (diameter of coflow is about 20 times the diameter of the outer annulus) [11]. The developement length is sufficiently long to obtain fully-developed turbulence at the burner exit. The development length is also short enough to avoid excessive decay of swirl [11]. The outer annulus is fed by the middle and upper plenums B, C in the burner. If the middle plenum (B) is used in isolation, the resulting outer annulus flow is axial. A variable degree of swirl can be introduced to the outer flow by passing a percentage of the overall outer annulus flow through the upper plenum (C) [11]. Flow straightening rings (H) are fitted to the inner and outer annulus close to the plenums supplying axial flow. The rings have several small through-holes arranged in a radially symmetric pattern, with major axes parallel to those of the annuli. Turbulence is generated by the changes in the sectional area as the flow passes through the holes, and the pressure drop across them is sufficiently high to ensure uniform flow [11].

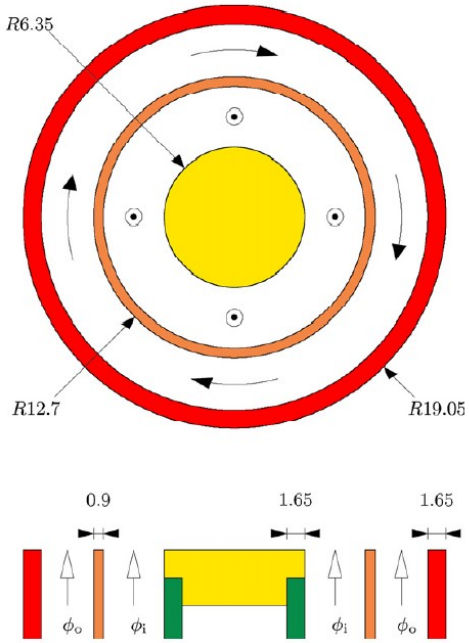

Figure 2.2. Plan view schematic of the exit geometry in the stratified swirl burner, showing a plan view and a cross section through the burner axis. (Image taken from [11].)

Figure 2.2 shows the top view of the burner and the flow directions of the premix for a swirling case. It also gives us the dimensions of the annuli and the annular walls. The bulk velocity in the outer annulus, $U_o = 18.7m/s$, is set at more than twice the value of the velocity in the inner annulus, $U_{\mathrm{i}} = 8.31m/s$, in order to generate substantial levels of shear between the two flows. Co-flow air is supplied around the outer annulus with a bulk velocity $U_{co-flow} = 0.4m/s$ to prevent the entrainment of ambient air. The Reynolds numbers (Re) derived from the bulk velocities and the exit geometry are $Re_{\mathrm{i}} = 5960$ for the inner annulus and $Re_o = 11,500$ for the outer annulus [11].

2.2 Operating Conditions

As mentioned earlier, in the present study , we are considering only the non-swirling cases of the burner. For that, we refer to Sweeney et al. [11] for the experimental values and operating conditions. For all stratification levels, the velocities are the same i.e. $U_o = 18.7m/s$, $U_{\mathrm{i}} = 8.31m/s$ and $U_{co-flow} = 0.4m/s$. Inlet temperature is set to $295K$ and 1 bar pressure. The stratification ratio, SR, defined as the ratio of the nominal equivalence ratio in the inner annulus to that in the outer, was varied from 1 for premixed cases to 3 for the most stratified case [11]. These cases are described as lean because the region of primary interest in the stratified flames is where the mean flame brush, defined as the location of peak temperature fluctuation, crosses the middle of the mixing layer as defined by the location where $\phi_g = 0.5(\phi_{\mathrm{i}} + \phi_o)$. The table below provides the details of the cases.

Table 2.1. Operating conditions considered in the current study [11].

Sr.No	Stratification Ratio	ϕ_{i}	ϕ_o	Name
1	1	0.75	0.75	SwB1
2	1	1	0.5	SwB5
3	3	1.125	0.375	SwB9

2.3 Flame Characteristics

Experimental data is provided by Sweeney et al. [11][23], Zhao et al. [24] and Euler et al. [25]. The Damkohler number is estimated to be between 0.89 and 1.24 and the Karlowitz number between 93 and 215 (Shown in Figure 2.3). Under these conditions, the flame falls into the thin reaction zone regime [16]. Significant levels of stratification are achieved within the flame front. Favre averaged results reveal elevated equivalence ratio levels within the recirculation zone for the premixed case. This is attributed to the combined effects of preferential transport of hydrogen away from the flame front near to the burner exit and the accumulation of CO_2 within the recirculation zone, which increases the calculated equivalence ratio based on the main species [11].

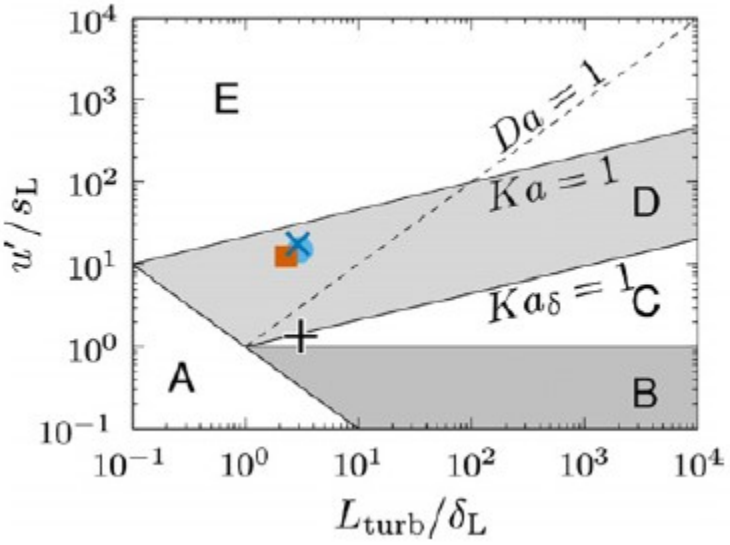

Figure 2.3. Modified Borghi Plot, Relevent case (with no swirl) marked with a cross. (Image taken from [11].)

Recirculation zones can be observed behind the bluff body, these help in stabilizing the flame. The length of the recirculation zone in the premixed case, SwB1, is significantly longer than those in the stratified cases. Moreover, the length in SwB5 is slightly shorter than that in SwB9 [21]. Near-exit profiles of mean and fluctuating components of radial and axial velocities in non-reacting conditions are also shown to approximate boundary conditions

[11]. Figure 2.4 shows the mean and fluctuating velocity fields for non-reacting cases and cases with varying levels of stratification where r stands for the radial distance from the center.

2.4 Experimental Data

A good amount of experimental data is made readily available for the Cambridge Burner [23][11][24][25]. First, velocity characterization in the swirl burner was performed using two-dimensional particle image velocimetry (PIV), giving the velocity components in the axial and radial directions [11]. Pairwise two-component Laser Doppler Anemometry (LDA) measurements were also conducted, providing profiles of axial velocity, radial velocity, tangential velocity, and corresponding fluctuating velocities [24]. Near exit velocity ($z = 2$mm) data is available for non-reacting as well as reacting cases. Further data is available in increments of 10mm ($z = 10\text{mm}, 20\text{mm}$ and so forth). Favre and Reynolds averaged, and fluctuating data is available for different scalars (Temperature, Species, Equivalence ratio) at increments of 10mm for the reacting cases. Bluff body surface temperatures are available as a function of radial position.

As seen from the plots in Figure 2.5 and 2.6, the experimental data makes sense theoretically as the reactant mass fractions reduce almost linearly while the product mass fractions increase linearly with temperature. However, the experimental data is not exactly axisymmetric, which can be due to measurement uncertainties or deviations in the geometrical shape of the burner. This point will be discussed further while sharing the simulation results. The results of the simulation are verified using this available experimental data.

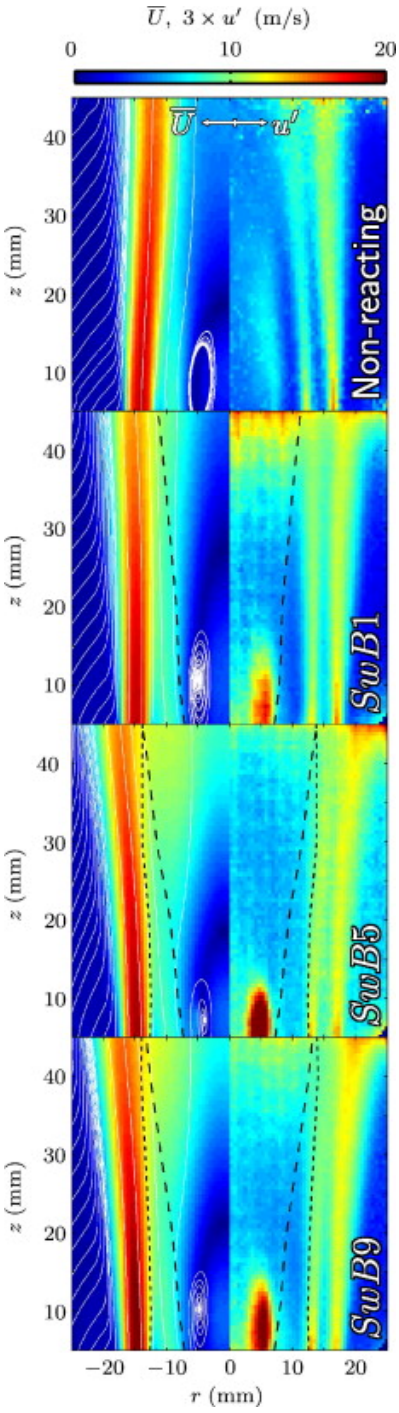

Figure 2.4. Mean ($r < 0$ mm) and fluctuating ($r > 0$ mm) velocities for non-reacting (top) and reacting conditions corresponding to cases SwB1, SwB5, and SwB9. (Image taken from [11].)

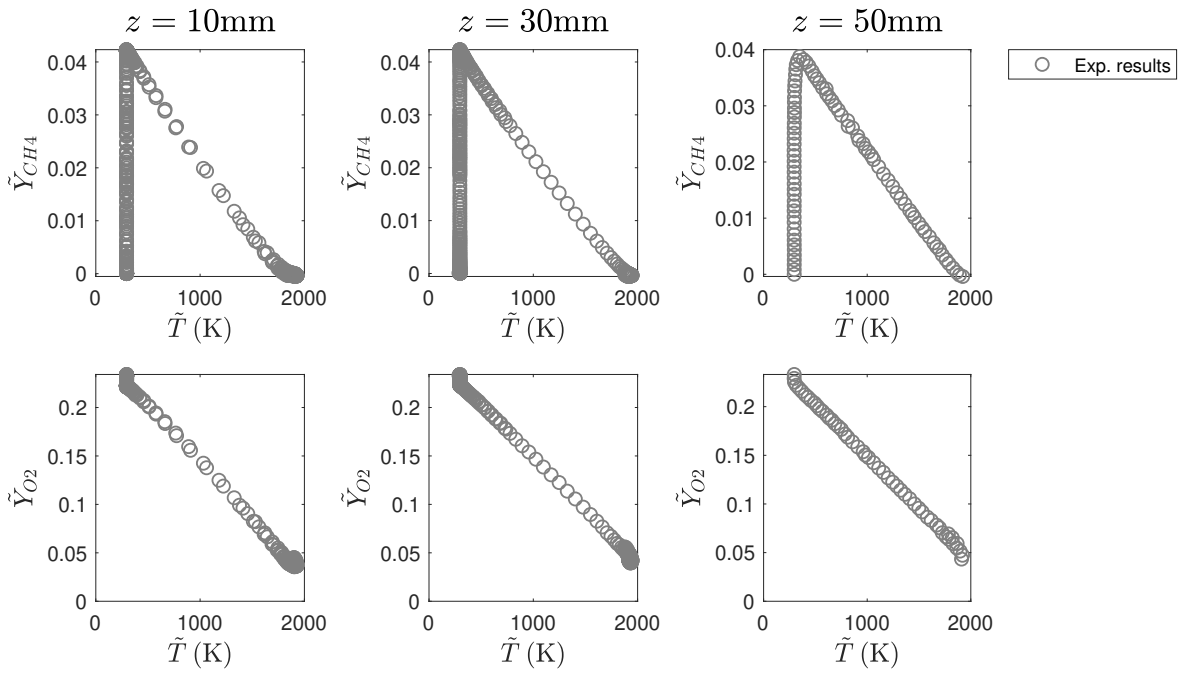

Figure 2.5. Plots of experimental mean CH4 and O2 mass fractions against mean temperature data [11].

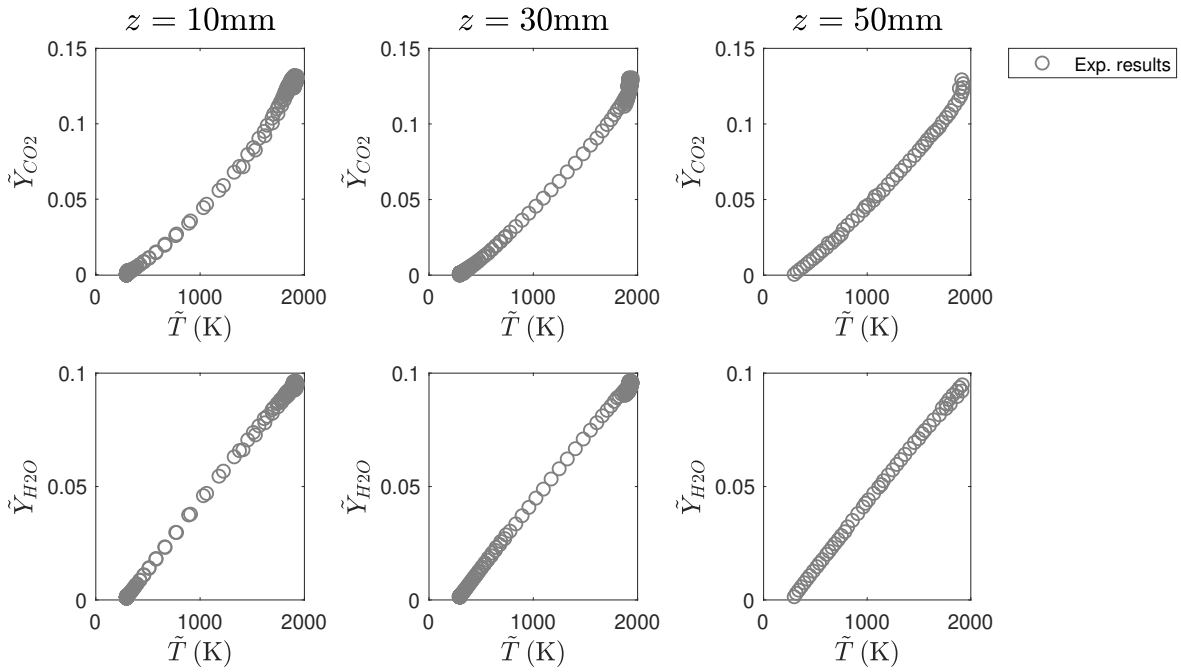

Figure 2.6. Plots of experimental mean CO2 and H2O mass fractions against mean temperature data [11].

3. NUMERICAL AND PHYSICAL MODELS

In this chapter, we describe the numerical and physical models used in this study. Few of the models are already present in Ansys FLUENT [13] such as the Reynolds stress model [26] for turbulence and the PDF method. Mixing models by Kuan et al. [27] and Kuran et al. [28] are coded in as User Defined Functions (UDFs) [29] which are C programs that can be compiled and hooked to the FLUENT case. Even though few of the models are present and ready to use as is, it is essential to have a good physical and mathematical understanding of the models to apply them to various cases.

3.1 Turbulence models

The Navier-Stokes (N-S) equations govern the flow of a fluid, including the velocity and pressure fields. These equations are highly non-linear, which makes them complicated to solve, and hence various numerical methods are employed to reduce the computational costs. In turbulent flows, flow quantities can be split into the mean and fluctuating portions. Averaging the resultant equations gives the Reynolds-averaged Navier–Stokes (RANS) equations, which govern the mean flow. Because of the non-linearity of the N-S equations, the non-linear term $-\rho\overline{u_i' u_j'}$ is still present in the RANS equation which comes from the convective acceleration. This term is called the Reynolds stress, R_{ij} and this requires modeling. [30]. For this, different kinds of closure models are used, the most common being modeling for the eddy viscosity ν_t. Popular eddy-viscosity based models like the k–ε model and the k–ω models have a few drawbacks in complex flows due to the use of the eddy-viscosity hypothesis in their formulation. In such flows, Reynolds stress equation models (RSM) offer much better accuracy [30].

The RSM closes the Reynolds-averaged Navier-Stokes equations by directly solving transport equations for the Reynolds stresses, with an equation for the turbulent dissipation rate ε. Since the RSM directly solves for the stresses, it generally has better accuracy for cases with rapid fluctuations of strain rate [31]. However, the limitations exist in the models used for the closure of the R_{ij} transport equations. In FLUENT, the exact transport equation for Reynolds Stress ($\rho\overline{u_i' u_j'}$) is formulated as

$$\underbrace{\frac{\partial}{\partial t}(\rho\overline{u_i' u_j'})}_{\text{Local Time Derivative}} + \underbrace{\frac{\partial}{\partial x_k}(\rho u_k \overline{u_i' u_j'})}_{C_{ij}\equiv \text{ Convection}} = P_{ij} + \phi_{ij} + \varepsilon_{ij} + D_{T,ij} + D_{L,ij} + G_{ij}, \tag{3.1}$$

where,

- $P_{ij} \equiv -\rho\Big(\overline{u_i' u_j'}\frac{\partial u_j}{\partial x_k} + \overline{u_j' u_k'}\frac{\partial u_i}{\partial x_k}\Big) \equiv$ Stress Production
- $\phi_{ij} \equiv \overline{p\Big(\frac{\partial u_i'}{\partial x_j} + \frac{\partial u_j'}{\partial x_i}\Big)} \equiv$ Pressure Strain
- $\varepsilon_{ij} \equiv 2\mu\overline{\frac{\partial u_i'}{\partial x_k}\frac{\partial u_j'}{\partial x_k}} \equiv$ Dissipation
- $D_{T,ij} \equiv -\frac{\partial}{\partial x_k}[\rho\overline{u_i' u_j' u_k'} + \overline{p(\delta_{kj}u_i' + \delta_{ik}u_j')}] \equiv$ Turbulent Diffusion
- $D_{L,ij} \equiv \frac{\partial}{\partial x_k}[\mu\frac{\partial}{\partial x_k}(\overline{u_i' u_j'})] \equiv$ Molecular Diffusion
- $G_{ij} \equiv -\rho\beta(g_i\overline{u_j'\theta} + g_j\overline{u_i'\theta}) \equiv$ Buoyancy Production

Here, C_{ij}, P_{ij}, and $D_{L,ij}$ do not require any modeling, but $D_{T,ij}$, ϕ_{ij}, G_{ij}, and ε_{ij} need to be modeled to close the equation [31]. The FLUENT theory guide [31] gives us a detailed explanation of how these terms are modeled along with the constants. The transport equation for scalar dissipation rate ε is the same as the one used in the k- ϵ model, for which the turbulent viscosity, μ_t is modeled as [31]:

$$\mu_t = \rho C_\mu \frac{k^2}{\epsilon}, \tag{3.2}$$

where $C_\mu = 0.09$ [31].

Standard wall functions were used in the current simulations because we are modeling an open flame but enhanced wall function models are also available. A comparison is shown in the results which shows that the performance of the RSM model is better than other turbulence models for this case.

3.2 Transported PDF Method

A transport equation for the single-point, joint PDF can be derived. This PDF, denoted by f, can be considered to represent the fraction of the time that the fluid spends at each species, temperature and pressure state, i.e., f has $N+2$ dimensions. This transport equation helps in solving the closure problem for the reactive scalar source term [31]. The joint PDF can be resolved by solving the PDF transport equation:

$$\frac{\partial}{\partial t}(\rho f) + \frac{\partial}{\partial x_{\mathrm{i}}}(\rho u_{\mathrm{i}} f) + \frac{\partial}{\partial \Psi_k}(\rho S_k f) = -\frac{\partial}{\partial x_{\mathrm{i}}}\Big[\rho \langle u''_{\mathrm{i}} | \Psi \rangle f\Big] + \frac{\partial}{\partial \Psi_k}\Big[\rho \Big\langle \frac{1}{\rho}\frac{\partial J_{\mathrm{i},k}}{\partial x_{\mathrm{i}}}\Big| \Psi \Big\rangle f\Big], \tag{3.3}$$

where,

- f = Favre joint PDF of composition [31]
- ρ = mean fluid density [31]
- u_{i} = Favre mean fluid velocity vector [31]
- S_k = reaction rate for specie k [31]
- Ψ = composition space vector [31]
- u''_{i} = fluid velocity fluctuation vector [31]
- $J_{\mathrm{i},k}$ = molecular diffusion flux vector [31]

The notation $\langle \dots \rangle$ denotes expectations, and $\langle A|B \rangle$ is the conditional probability of event A, given event B occurs [31].

Since the reaction term is closed, terms that need modeling in the transport equation are the two terms on the right. These terms are the turbulent scalar flux and the molecular mixing term [31]. The modeling of both these terms is explained in the FLUENT theory guide [31], and while the modeling of the scalar flux is fairly straight forward, modeling of the mixing term plays a major role is the performance of the PDF method [31]. The transport

equation for the PDF is solved using Lagrangian Monte-Carlo methods. This involves the assumption of particles that move randomly in physical space, and also in the composition space due to mixing and chemical reactions. This has also been the basis of a few mixing models for closing the PDF transport equation.

3.3 Mixing Models

Various mixing models were implemented over the course of the study to find what suits the case. These can broadly be classified into pre-existing models in FLUENT and mixing models implemented to enhance the performance of the existing models. Both these categories are briefly discussed in this chapter.

3.3.1 Fluent Mixing models

There are 3 mixing models provided by FLUENT for molecular mixing, Modified curl model [32], IEM model [33]and the EMST model. In this study, we look at the IEM model and the Modified Curl (MCurl) model.

Modified Curl Model

MCurl model is a particle interaction model based on Curl's model (Curl, 1963) [32]. Random pairs of particles (represented by p and q) are selected and their compositions are altered to be closer to their mean composition proportional to a uniform random number ξ [31]. The composition is updates as shown:

$$\phi_p^1 = (1-\xi)\phi_p^0 + \xi\frac{(\phi_p^0 m_p + \phi_q^0 m_q)}{(m_p + m_q)}. \tag{3.4}$$

$$\phi_q^1 = (1-\xi)\phi_q^0 + \xi\frac{(\phi_p^0 m_p + \phi_q^0 m_q)}{(m_p + m_q)}. \tag{3.5}$$

Here, ϕ_p and ϕ_q are the composition vectors while m_p and m_q are the masses for particles p and q. State 0 is the initial state while state 1 is the updated state of the compositions.

IEM model

The Interaction by Exchange with the Mean (IEM) model was developed by Villermaux and Devillon in 1972. Here, the composition of all particles in a cell are moved a small distance toward the mean composition [31]:

$$\frac{\partial \phi}{\partial t} = -\frac{1}{2} C_\phi \frac{\varepsilon}{k} (\phi - \tilde{\phi}), \tag{3.6}$$

where,

- $\tilde{\phi}$ is the Favre mean-composition vector at the particle's location
- C_ϕ is the mixing constant (default = 2)

Mixing takes place in particles that are physically close to each other and the IEM model is relatively rough for it doesn't consider the localness in composition space.

3.3.2 Other mixing models implemented in this study

We tried implementing two other mixing models made for closing the mixing term in the PDF transport equation, the details of which are mentioned below.

Mixing timescale model for PDF method calculations(Kuan et al., 2003)

In cases where the Damkohler number (Da $= \tau_t/\tau_c$, where τ_t and τ_c are characteristic turbulence and chemical timescales, respectively) is one or greater than one, The chemical mixing frequency τ_c^{-1} is directly related to the closure for the scalar dissipation rate ($\tilde{\varepsilon}_c$) [27]:

$$\tau_c^{-1} = \frac{\tilde{\varepsilon}_c}{\tilde{c''^2}} = \frac{C_\phi}{2} \frac{\tilde{\varepsilon}}{\tilde{k}} = \frac{C_\phi}{2} \tau_t^{-1}. \tag{3.7}$$

Here, τ_t^{-1} is the turbulence mixing frequency given by $\frac{\tilde{\varepsilon}}{\tilde{k}}$ and c is a scalar quantity.

Transport equation for scalar dissipation rate:

$$\frac{\partial\langle\rho\rangle\tilde{\varepsilon}_c}{\partial t}+\frac{\partial\langle\rho\rangle\tilde{u}_1\tilde{\varepsilon}_c}{\partial x_1}=-\frac{\partial J_1^{\varepsilon_c}}{\partial x_1}+\left[C_{\varepsilon_{c1}}\frac{\tilde{\varepsilon}}{\tilde{k}}\frac{P}{\tilde{\varepsilon}}+C_{\varepsilon_{c2}}\frac{\tilde{\varepsilon}}{\tilde{k}}\frac{P_c}{\tilde{\varepsilon}_c}-C_{\varepsilon_{c3}}\frac{\tilde{\varepsilon}}{\tilde{k}}-C_{\varepsilon_{c4}}\frac{\tilde{\varepsilon}_c}{\tilde{c''^2}}\right]\times\langle\rho\rangle\tilde{\varepsilon}_c. \tag{3.8}$$

We assume that the growth of the scalar dissipation rate , left-hand side of the transport equation, is dominated by the local source term (first term in the right of the transport equation) [27]. The resulting reduced equation is:

$$\left[C_{\varepsilon_{c1}}\frac{\tilde{\varepsilon}}{\tilde{k}}\frac{P}{\tilde{\varepsilon}}+C_{\varepsilon_{c2}}\frac{\tilde{\varepsilon}}{\tilde{k}}\frac{P_c}{\tilde{\varepsilon}_c}-C_{\varepsilon_{c3}}\frac{\tilde{\varepsilon}}{\tilde{k}}-C_{\varepsilon_{c4}}\frac{\tilde{\varepsilon}_c}{\tilde{c''^2}}\right]\simeq 0. \tag{3.9}$$

$$\frac{\tilde{\varepsilon}_c}{\tilde{c''^2}}=\underbrace{\frac{1}{C_{\varepsilon_{c4}}}\left[C_{\varepsilon_{c1}}\frac{P}{\tilde{\varepsilon}}+C_{\varepsilon_{c2}}\frac{P_c}{\tilde{\varepsilon}_c}-C_{\varepsilon_{c3}}\right]}_{C_1^*}\frac{\tilde{\varepsilon}}{\tilde{k}}. \tag{3.10}$$

The parameter C_1^* denotes the "constant" C_ϕ of corresponding mixing time-scale expressions [27]. In flows with reactive scalars, the equation for the scalar dissipation rate includes reaction specific terms in the form of correlations between scalar and reaction rate gradients [27].

$$\langle S_{\varepsilon_c}\rangle=2D_c\left\langle\frac{\partial c''}{\partial x_1}\frac{\partial S_c}{\partial x_1}\right\rangle. \tag{3.11}$$

Borghi and Mantel [34] show that the above term is of Ø(Da). Hence, in high-Damkohler-number flows, the contribution of the term is significant. Kuan et al. [35] derived an expression for the time-scale ratio as a function of integral and small-scale properties.

$$\tau_c^{-1} = \frac{\tilde{\varepsilon_c}}{c''^2} \propto \frac{\rho_u}{\langle\rho\rangle}\frac{u_L}{\nu_K}\frac{\tilde{\varepsilon}}{\tilde{k}}. \tag{3.12}$$

A disadvantage of Equation 3.12 is that if c is a passive scalar then the corresponding mixing time scale is zero [27]. and hence, Kuan et al. [35] derived a modification:

$$\tau_c^{-1} = \frac{\tilde{\varepsilon_c}}{c''^2} = \frac{C_\phi}{2}\left[1.0 + C_\phi^*\frac{\rho_u}{\langle\rho\rangle}\frac{u_L}{\nu_K}\right]\frac{\tilde{\varepsilon}}{\tilde{k}}, \tag{3.13}$$

where $C_\phi^* = 1.2$.

Mixing timescale model for PDF simulations of turbulent premixed flames (Kuron et al., 2017)

Reactive scalar mixing rates in turbulent premixed flames depend on the local state of both the flow turbulence and the chemical reactions, which can be characterized by the Dahmkoler number [28]. The exact transport equation for Favre-averaged scalar dissipation rate of the progress variable, χ_c, can be approximated as [36]:

$$\overline{2\rho\chi_c\frac{\partial u_1}{\partial x_1}} - 2\overline{\rho\Gamma_c}\left(\frac{\partial c''}{\partial x_j}\frac{\partial \tilde{u}_j''}{\partial x_k}\frac{\partial c''}{\partial x_k}\right) + 2\left(\overline{\frac{\partial c''}{\partial x_k}\frac{\partial}{\partial x_k}}\right) - \overline{2\rho\left(\Gamma_c\frac{\partial^2 c''}{\partial x_j x_k}\right)^2} \approx 0. \tag{3.14}$$

The terms in the above equation require closure so a new mixing timescale model was proposed which considered flamelet controlled as well as turbulence controlled mixing [28]. Assuming passive scalar mixing, Borghi and Mantel [34] proposed a model that is proportional to the turbulence timescale :

$$\Omega_t = \frac{\tilde{\chi_\phi}}{\tilde{\phi''^2}} = C_\phi\tau_{turb}^{-1}. \tag{3.15}$$

where,

- Ω = Favre averaged mixing rate
- $\tilde{\chi_\phi}$ = Favre averaged scalar dissipation rate
- $\tilde{\phi''}$ = Favre averaged scalar variance
- C_ϕ = mechanical-to-scalar timescale ratio
- τ_{turb} = turbulence timescale

For the limiting assumption of laminar flamelets amidst a turbulent flowfield, the mixing rate can be defined as:

$$\Omega_f = \frac{\tilde{\chi_c}}{\tilde{c''^2}} = \int_0^1 \langle \chi_c | \zeta \rangle \tilde{P}_c(\zeta) d\zeta / \tilde{c''^2}, \tag{3.16}$$

where,

- $\tilde{P}_c(\zeta)$ = Favre-averaged probability density function of the progress variable
- ζ = sample space variable

In practical conditions, neither of the assumptions are valid throughout the flow field. Some state between the two limiting assumptions is required. For this, the segregation factor, η was defined:

$$\eta = \frac{\tilde{c''^2}}{[\tilde{c}(1-\tilde{c})]}. \tag{3.17}$$

The combined timescale model is formulated as:

$$\Omega_{hybrid} = (1-\eta) C_\phi \tau_{turb}^{-1} + \eta \int_0^1 \langle \chi_c | \zeta \rangle \tilde{P}_c(\zeta) d\zeta / \tilde{c''^2}. \tag{3.18}$$

4. SIMULATION DETAILS

This chapter briefly discusses the simulation details and setup used. Since the Cambridge burner is made of annular inlets, an axisymmetric two-dimensional simulation is set up. Ansys Design Modeler and Ansys Fluent Meshing tool is used to generate a simple two-dimensional mesh for the flame domain. The aim is to ensure grid independence in the region of interest while maintaining a low computational cost. The final grid shown in Figure 4.1 consists of 35642 nodes. The pressure-based solver was used to enable transported

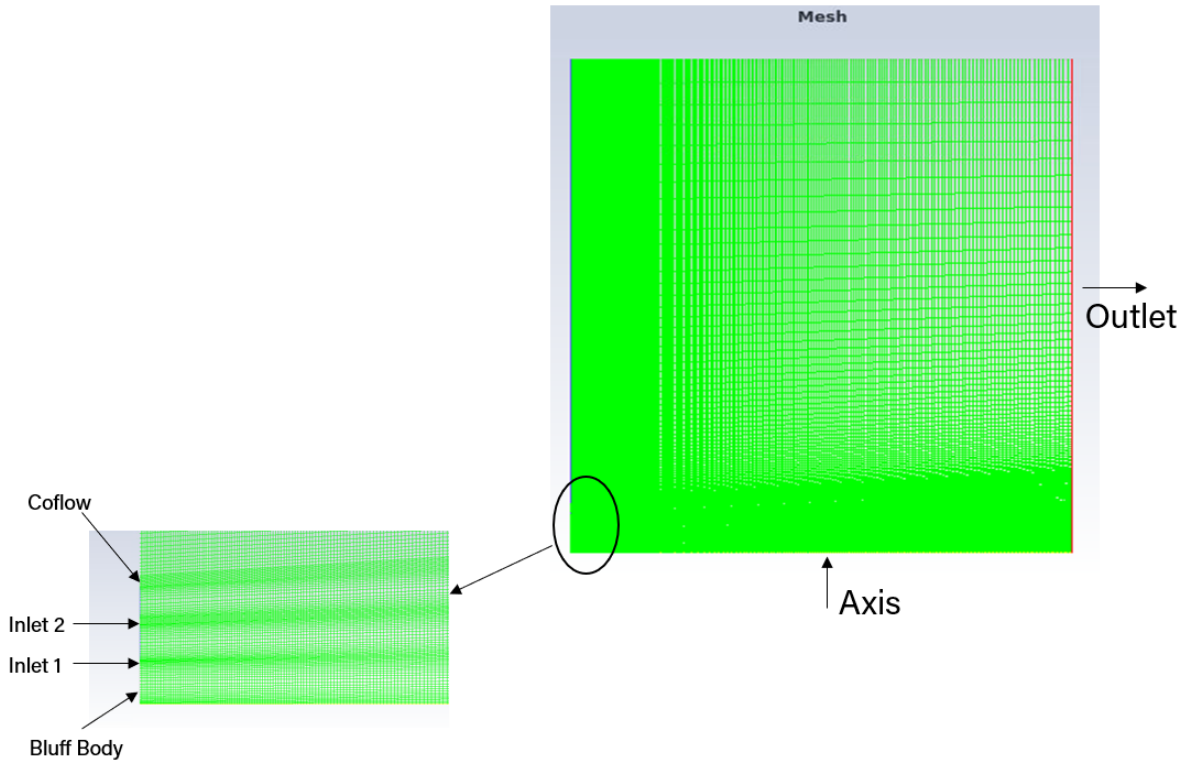

Figure 4.1. Computational Domain spanning 180mm axially and 190mm radially. The grid consist of 35642 nodes. Zoomed in section shows the near-inlet region.

PDF modeling. Various monitors at different locations are used for observing the change in properties w.r.t. iterations to ensure convergence.

4.1 Boundary Conditions

- For the two premixed fuel-air inlets, near inflow non-reacting experimental conditions ($z = 2$mm) are imposed on turbulence generated by setting up two 253mm pipes (as shown in Figure 4.2) to allow the flow to be fully developed.
- Mass flow of methane and air is set according to the operating equivalence ratio for each premix inlet.
- No turbulence is generated for the co-flow and the inlet velocity of 0.4m/s is imposed with air as the fluid.
- A no-slip boundary condition is imposed on the bluff-body wall.

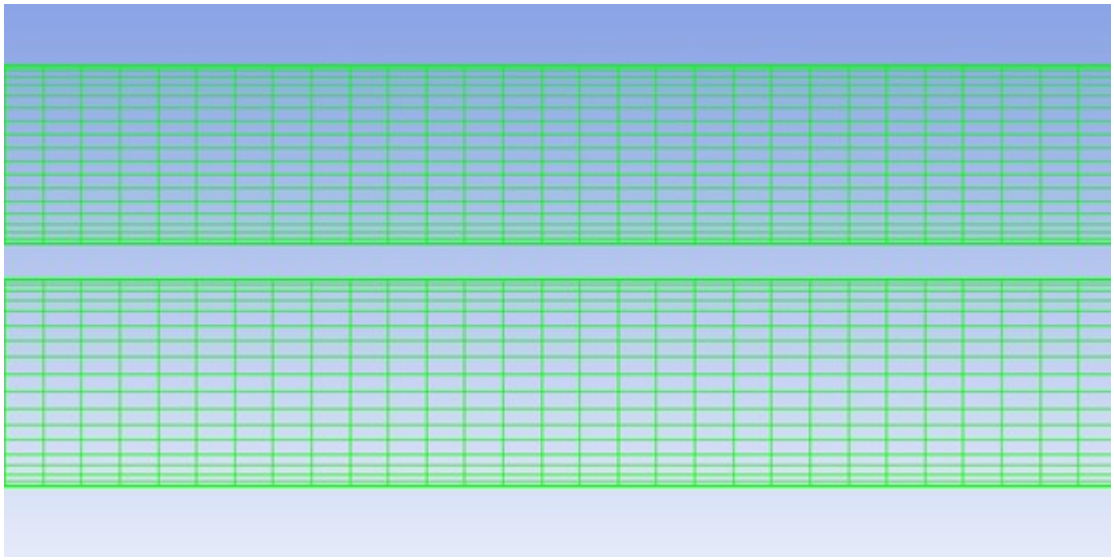

Figure 4.2. Computational mesh used for simulating pipes generating fully developed inlet turbulence.

4.2 Turbulence model

For the given operating conditions, the five-equation Reynold's Stress model preforms better for modeling the vectors within the recirculation zone and is hence chosen despite the

higher computational cost. Its performance is compared with other turbulence models and the results are presented in a later section.

4.3 Chemical Mechanism

After testing multiple common chemical reaction mechanisms, a 17-species skeletal mechanism for lean $CH_{4/}O_2$ combustion which is based on GRI 1.2 is chosen [37]. The mechanism was used in FLUENT as a CHEMKIN input which is a chemical reaction software tool embedded in FLUENT to read chemical mechanisms.

4.4 Combustion model

We started this study with the goal of using the PDF method for stratified combustion, but this choice can be justified as shown in the results where the predictions obtained from this are compared with predictions obtatined by using the Laminar Chemistry Model [31] and the Eddy Dissipation Concept (EDC) model [31]. Different mixing models and constants were tried to see which suits the problem. Details of the combustion models and mixing models are discussed in the previous section and the comparison results will be shown in the next section.

5. RESULTS AND DISCUSSIONS

In this chapter, we discuss the results obtained and compare them with the experimental values. We also compare different models/methods to see what works better for our case and discuss the reasons for the same. We run an initial simulation to see where we stand on the SwB1 case. At the time, we were more concerned with the accuracy of predictions within the recirculation zone. The biggest issues we have with our initial simulation was the under prediction of axial velocity in the recirculation zone and the underprediction of temperature and other scalars in the recirculation zone (as shown in the figure). Another issue was that we did not anticipate the lack of axisymmetry in the results. We also did not observe the fluctuation results and as mentioned earlier, our focus was on the velocity and scalar results. This was taken as the starting point and various measures were taken to overcome these challenges. In Figure 5.1 and further figures showing simulation results compared with experimental, r stands for the radial distance from the axis of the burner in mm. z stands for axial distance from the burner entrance plane in mm.

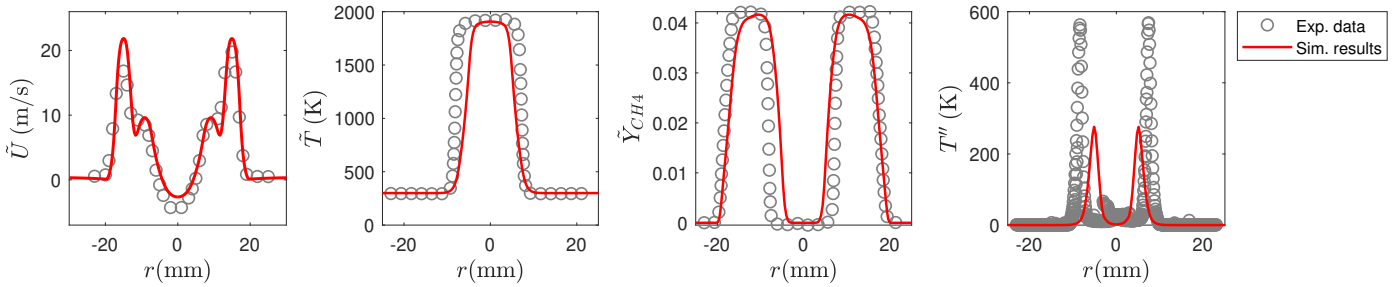

Figure 5.1. Initial simulation results for SwB1 at $z = 10$mm. From left to right: axial velocity, static temperature, mean CH_4CH4 mass fraction, and RMS temperature.

5.1 Effect of Boundary Conditions

One of the first attempts to better the solution is to modify the inlet boundary conditions (BC). The initial BC is obtained by generating a fully developed turbulence profile using two 253mm pipes, same as the development length in the burner. For this, the near exit

velocity values in non-reacting case are used as an input and turbulence was developed. This obtained profile is modified using trial and error methods to obtain a profile which improves the near exit results. In Figure 5.2, "Profile A" is the initial profile and "Profile B" is the modified profile. As seen, the major change is in the radial velocity profile at the mixing plane, the reason for which may be possible deviations in the geometrical shape of the burner which may cause the lack of asymmetry in the experimental values. The results of these small changes are also shown in Figure 5.3. The difference is significant to the velocity field but does not make much difference to the scalars. This was done to improve the flow field results within the recirculation zone.

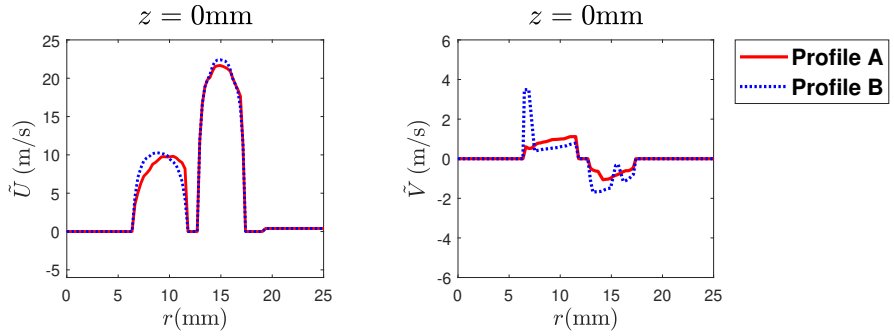

Figure 5.2. Changes made to the boundary profile for SwB1. "Profile A" stands for near exit profile in non-reacting case with turbulence, "Profile B" stands for the modified profile.

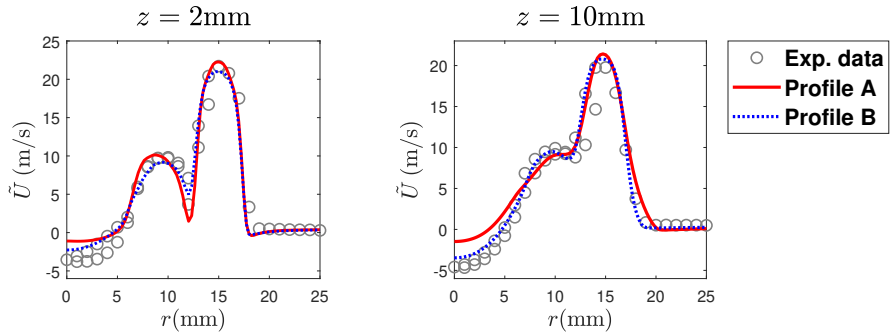

Figure 5.3. Near exit results of changes made to the boundary profile. "Profile A" stands for near exit results with Profile A as the boundary velocity profile, "Profile B" stands for near exit results with the modified profile as the boundary velocity profile.

5.2 Grid dependency for SwB1

A Grid dependence test is conducted which greatly helped with the scalar values. The three kinds of grid compared here refer to near exit grid quality and then the entire grid was refined two times to ensure grid independence. This study was conducted about the same time as the boundary condition study which is why the results here are with the older BC. This study just shows the dependence of the values on the grid. The "fine" grid shown in the results is picked to continue with the study. The near exit $\Delta = 0.3mm$ in both the x and y directions was found to be ideal to ensure independence. Figures 5.4 and 5.5 show the grid dependence.

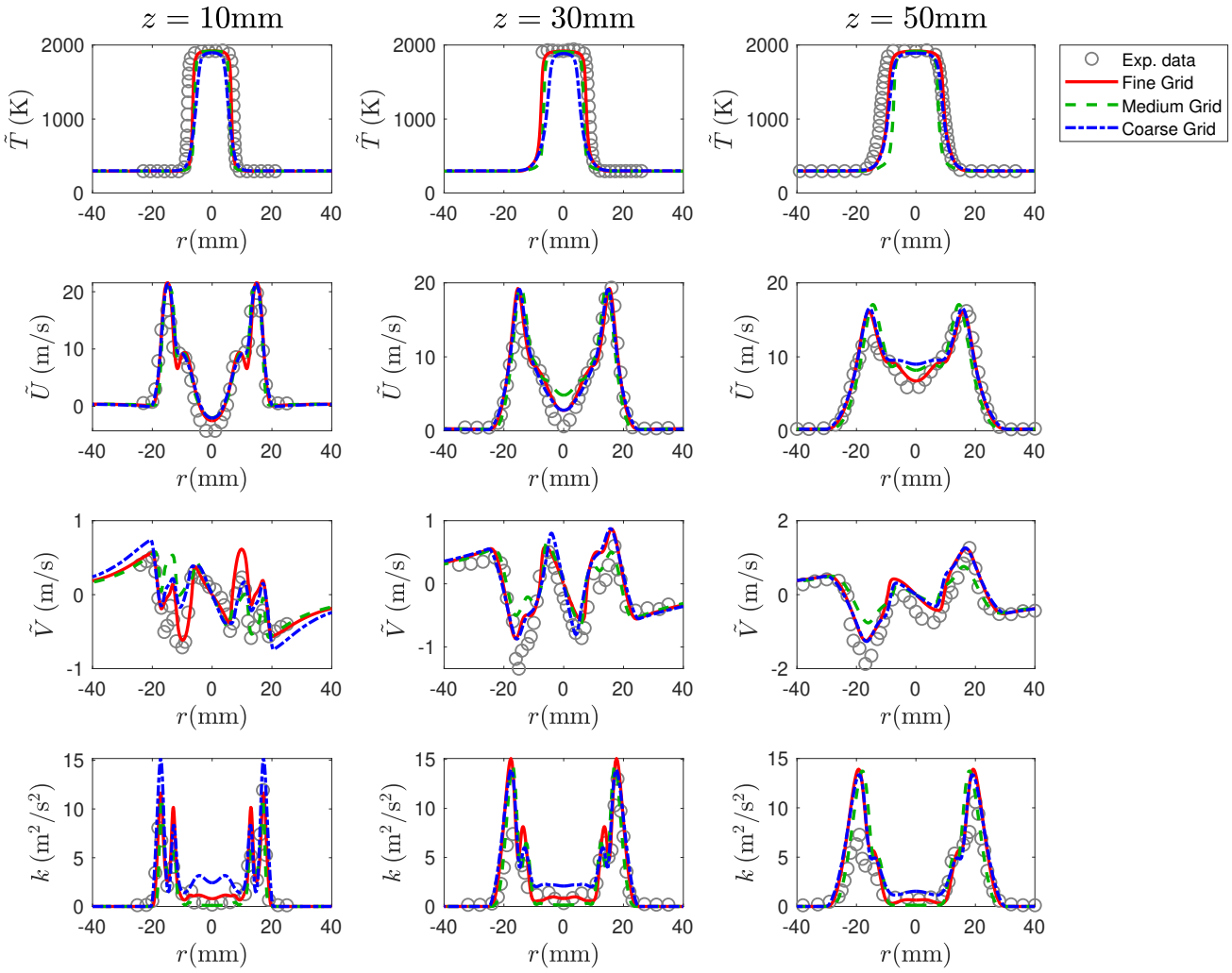

Figure 5.4. Radial profiles of (top to bottom) mean static temperature, axial velocity, radial velocity and turbulent kinetic energy showing the dependence of the values on the grid at different axial locations (left to right).

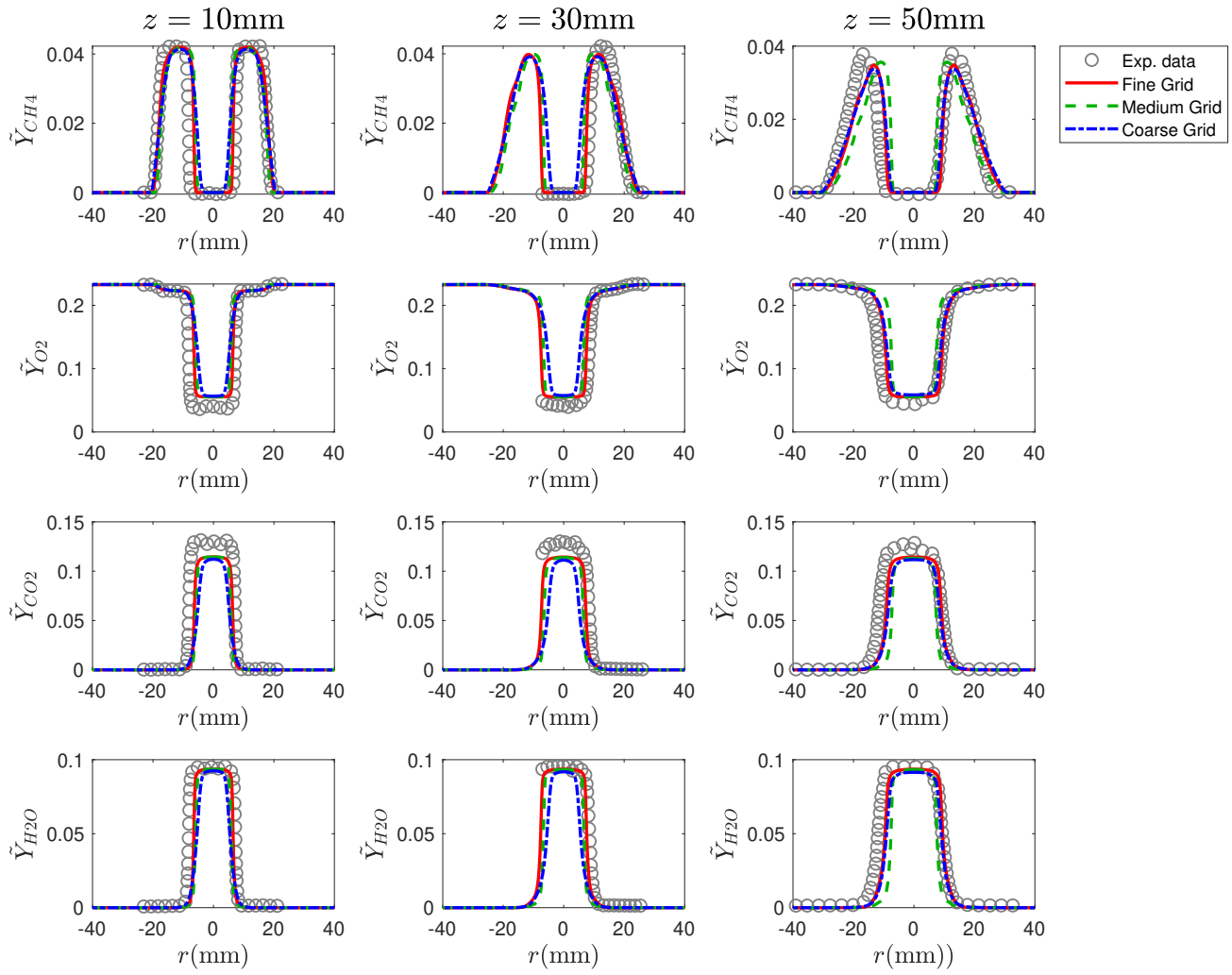

Figure 5.5. Radial profiles of (top to bottom) mean mass fractions of CH_4, O_2, CO_2, and H_2O and the dependence of their values on the grid at different axial locations (left to right).

5.3 Comparison of different turbulence models

SwB1 is used as a baseline case and the models and ideas are tested on this case and then extended to the stratified cases, SwB5 and SwB9 later. This section compares the Reynolds stress model (RSM) to standard k-ε and k-ω SST models. The results show a clear distinction towards the performance RSM model as shown in the figures below. In Figure 5.6, we can see how the prediction of velocity is much more accurate by the RSM model. In Figure 5.7, we see that the prediction of scalar means is similar for all the models, while we see in Figure 5.8 and Figure 5.9 that the RSM model slightly improves the fluctuation predictions. This trend is consistent in all the locations. The combustion model used for this comparison is the PDF method. As it can be seen, most of the mean values as well as the vectors are captured quite accurately already. The RMS values make sense qualitatively but are highly under predicted and hence further efforts were put into understanding the issues. As mentioned earlier, the under-prediction of fluctuation values has been observed in the literature as well but there is no clear solution or reasoning obtained for the same yet.

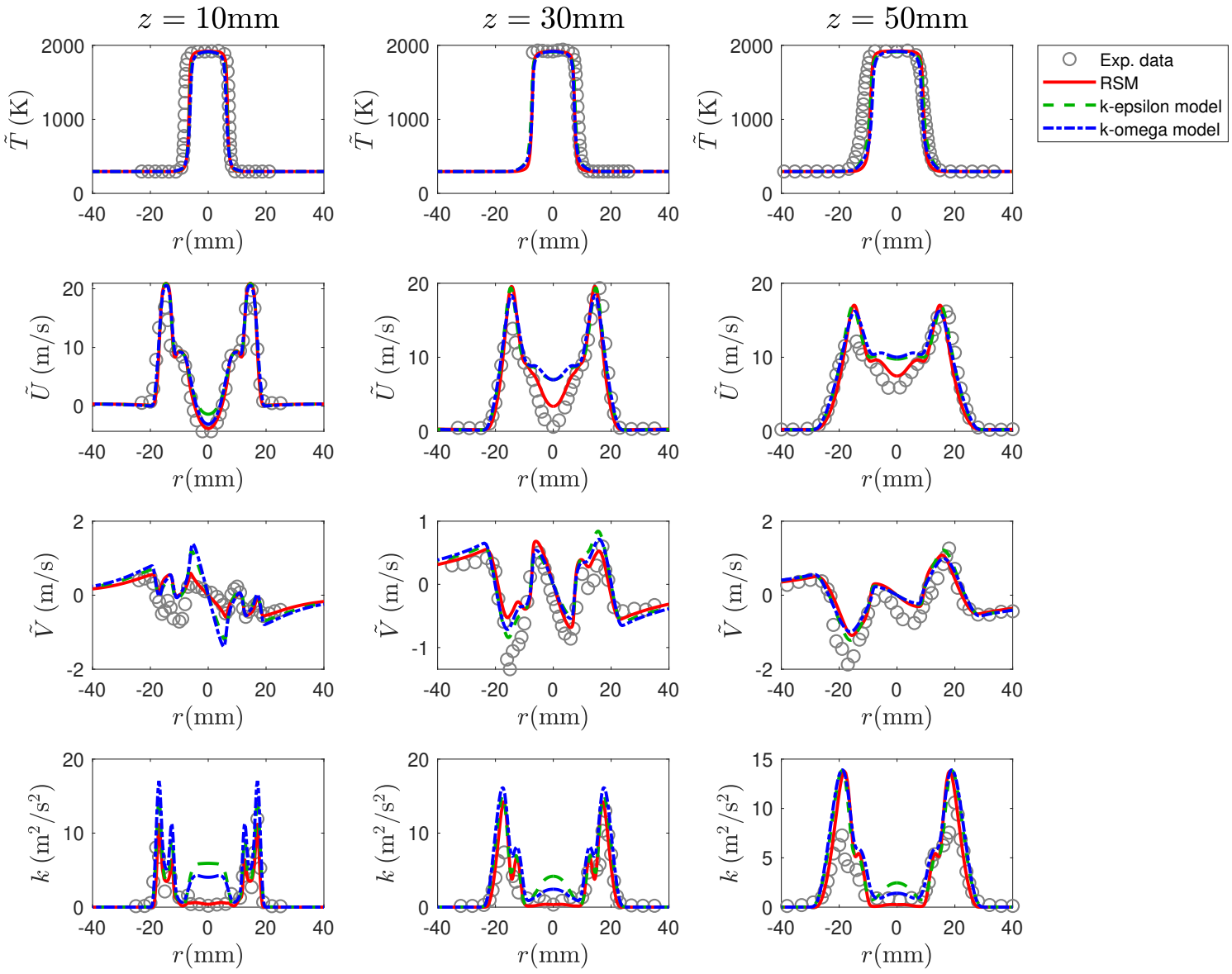

Figure 5.6. Performance comparison of different turbulence models on SwB1 plotted against experimental values at different axial locations. From top to bottom: Static Temperature, Axial Velocity, Radial Velocity, Turbulent Kinetic Energy.

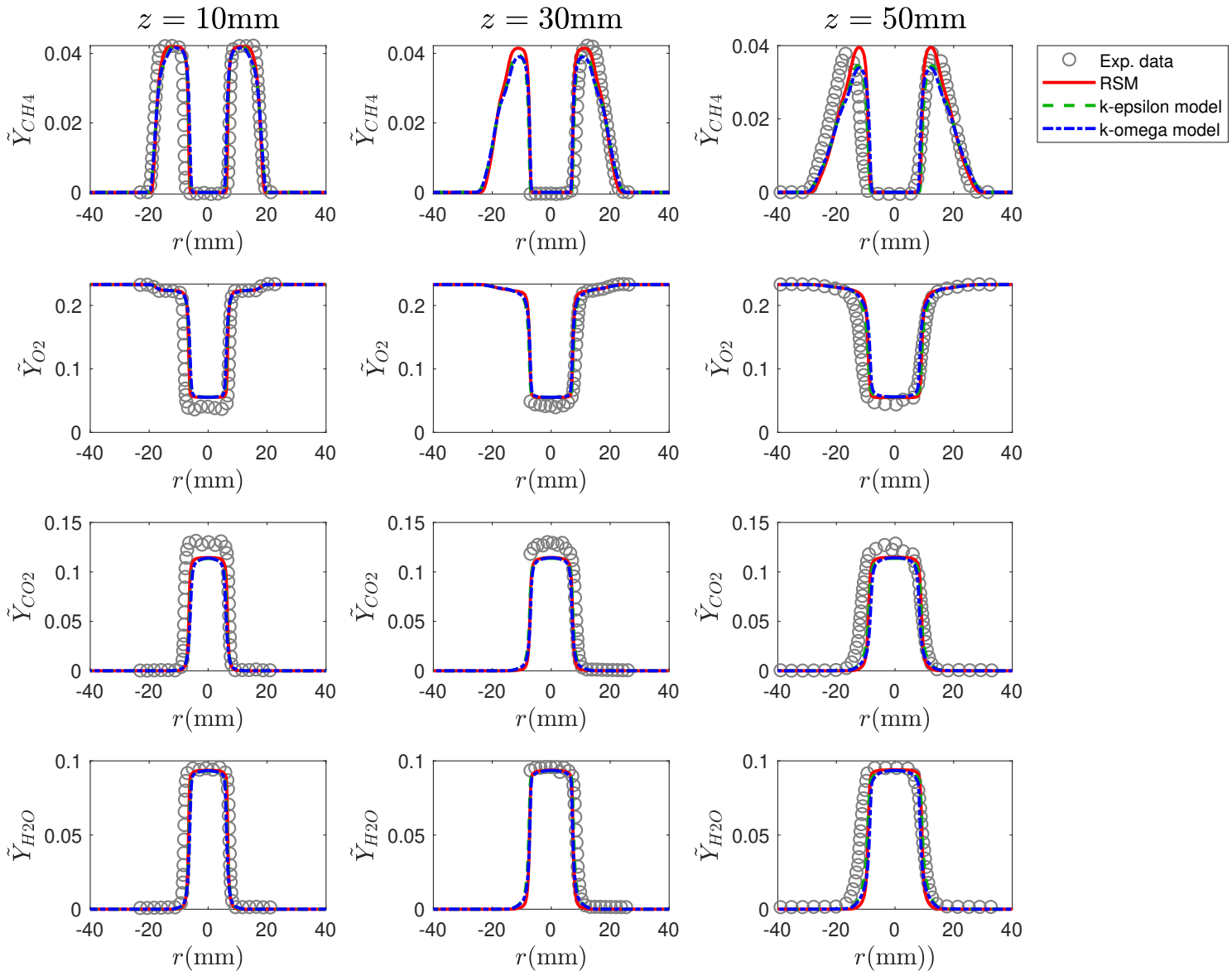

Figure 5.7. Performance comparison of different turbulence models on SwB1 plotted against experimental values at different axial locations. From top to bottom: Mean mass fractions of CH_4, O_2, CO_2, and H_2O.

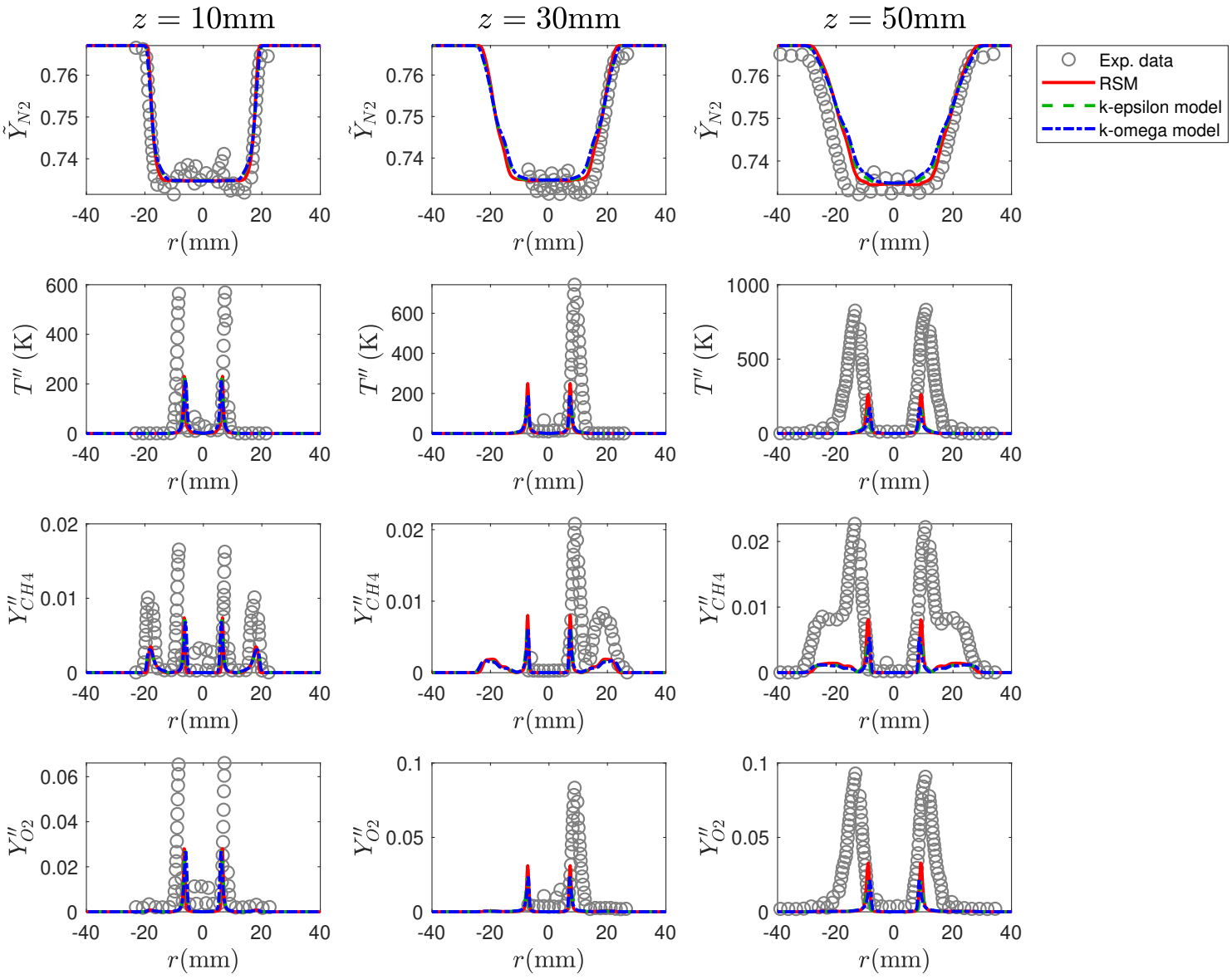

Figure 5.8. Performance comparison of different turbulence models on SwB1 plotted against experimental values at different axial locations. From top to bottom: Mean mass fraction of N_2, RMS Temperature, RMS mass fractions of CH_4, and O_2.

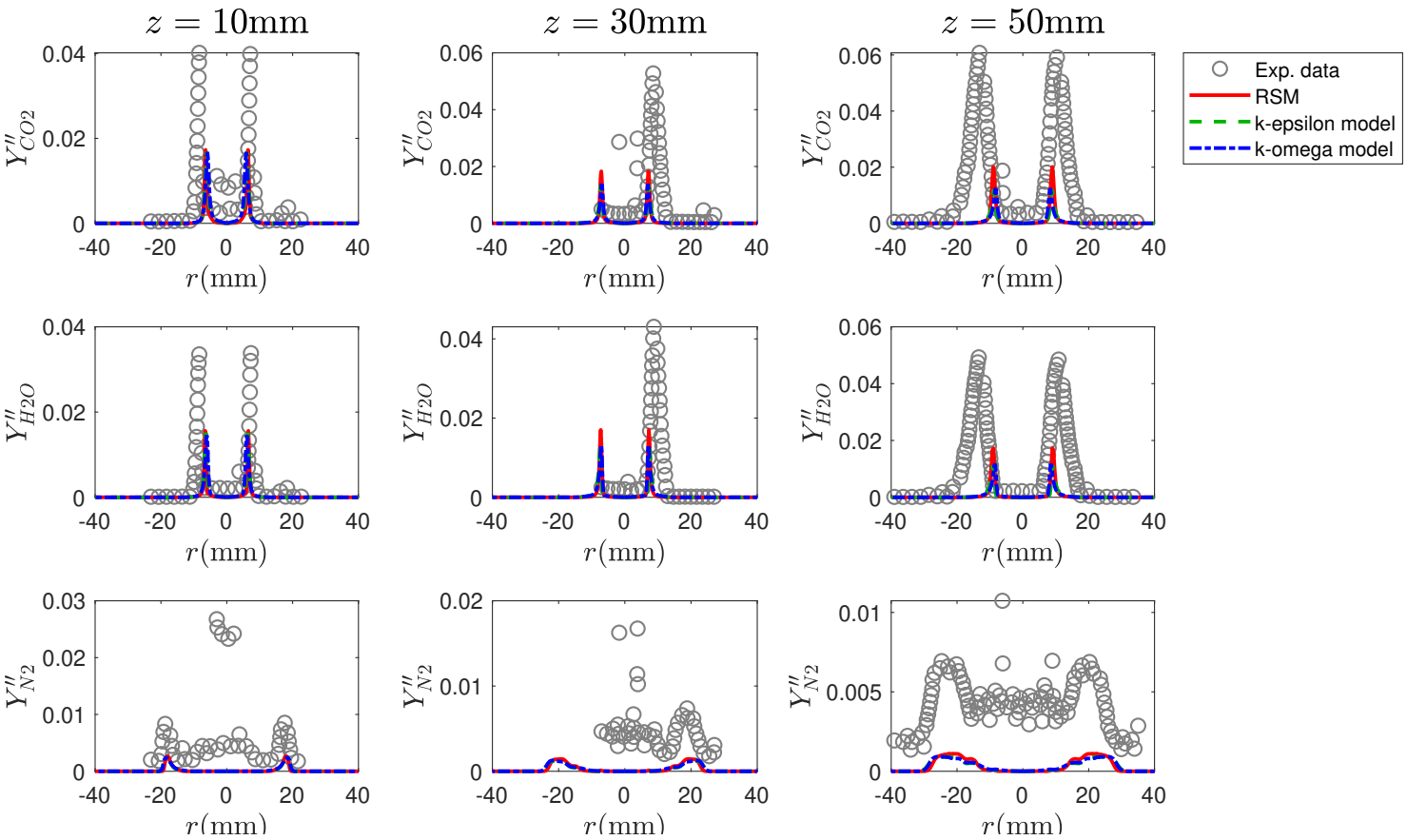

Figure 5.9. Performance comparison of different turbulence models on SwB1 plotted against experimental values at different axial locations. From top to bottom: RMS mass fractions of CO_2, H_2O, and N_2.

5.4 Comparison of Combustion models

This section gives a brief comparison of various combustion models and how they perform for this case. Our overall focus has been on the PDF method but this is good information to have to test the capabilities of different models and their pros and cons. Since the EDC and laminar chemistry models don't have the option to export RMS/fluctuation values, only the means have been compared. The RSM is used as the turbulence model for all cases in this comparison. As seen in Figure 5.10, the EDC model captures the axial velocity very well as compared to the other two. Both EDC and the laminar chemistry model, however, over-predict the temperature near the axis while the PDF method does a better job of capturing it. Overall, both qualitatively and quantitatively, the composition PDF method outperforms the other two in terms of suitability for the case as well as agreement of results with experimental. Figure 5.11 shows the comparison of different combustion models and their accuracy of predicting mean compositions of various species.

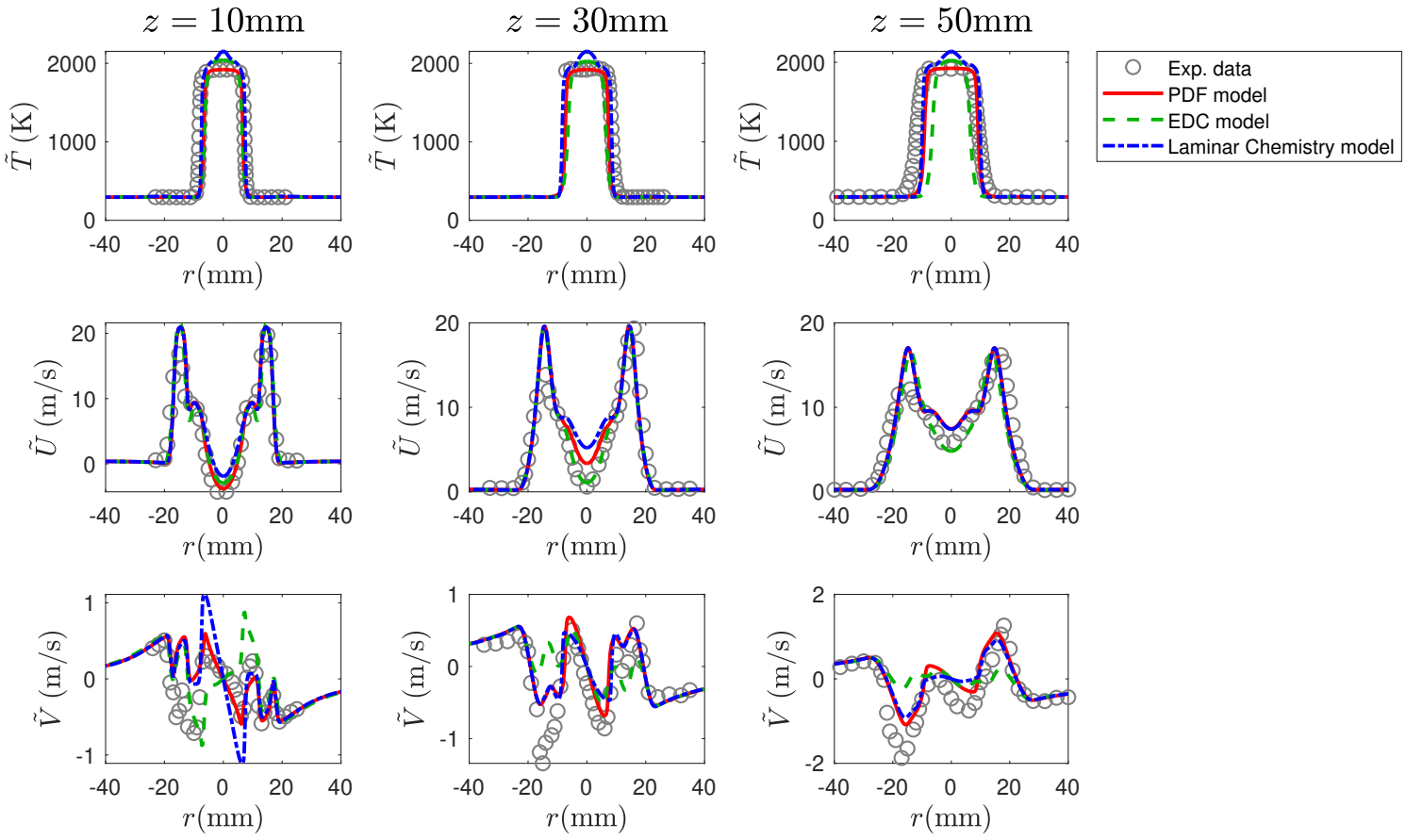

Figure 5.10. Comparison of results obtained from the PDF transport method compared with other combustion models on SwB1 at different axial locations. From top to bottom: Static Temperature, Axial Velocity, Radial Velocity.

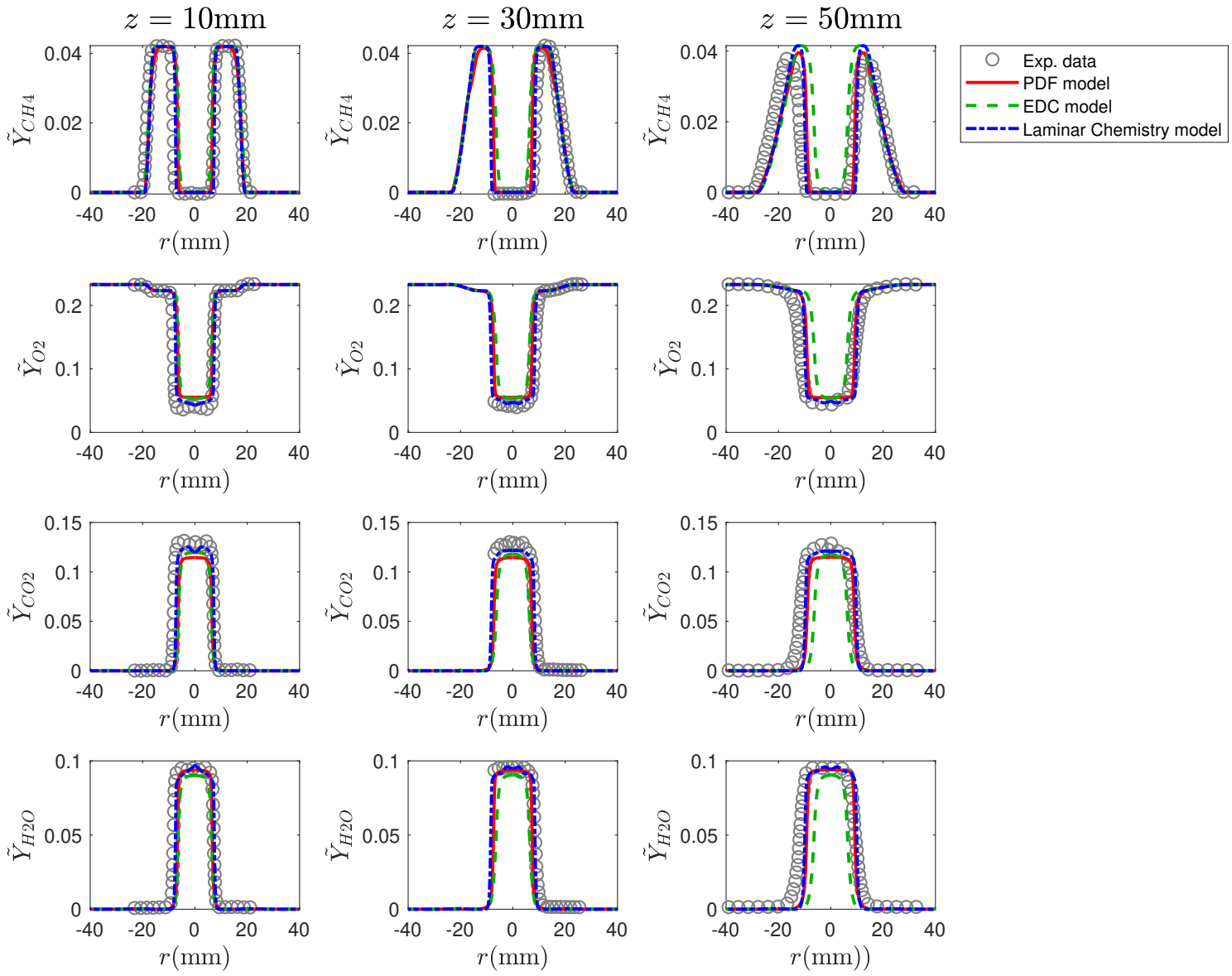

Figure 5.11. Comparison of results obtained from the PDF transport method compared with other combustion models on SwB1 at different axial locations. From top to bottom: Mean mass fractions of CH_4, O_2, CO_2, and H_2O.

5.5 Sensitivity to mixing constant (C_ϕ) Values

For all the results shown so far, the IEM mixing model was used along with very high value of mixing constant (essentially infinity) which gives good results for the mean field but the fluctuation values were much lower than expected. One parameter that affects fluctuations is the mixing and hence the mixing constant. The value of the mixing constant is progressively reduced and its effect on the results is observed.

It is observed that upto $C_\phi = 32$, the mean flow field is still captured well, and there is a slight improvement in the agreement of the rms values with the experimental. Once we go below this value, i.e. $C_\phi = 16$ and so on, there is significant detriment in the mean as well as rms results. If we look at the mean temperature profile in Figure 5.12, we can clearly see the decrease in performance at $z = 30$mm and $z = 30$mm. Similarly, in Figure 5.13 we can observe this decrease as we move downstream. In Figures 5.14 and 5.15, we can see the effects of reducing C_ϕ on the predicted fluctuations.

Since this study did not help with solving the issue at hand, other methods such as changing the mixing model and implementing new mixing models are employed with the hope of narrowing down the issue.

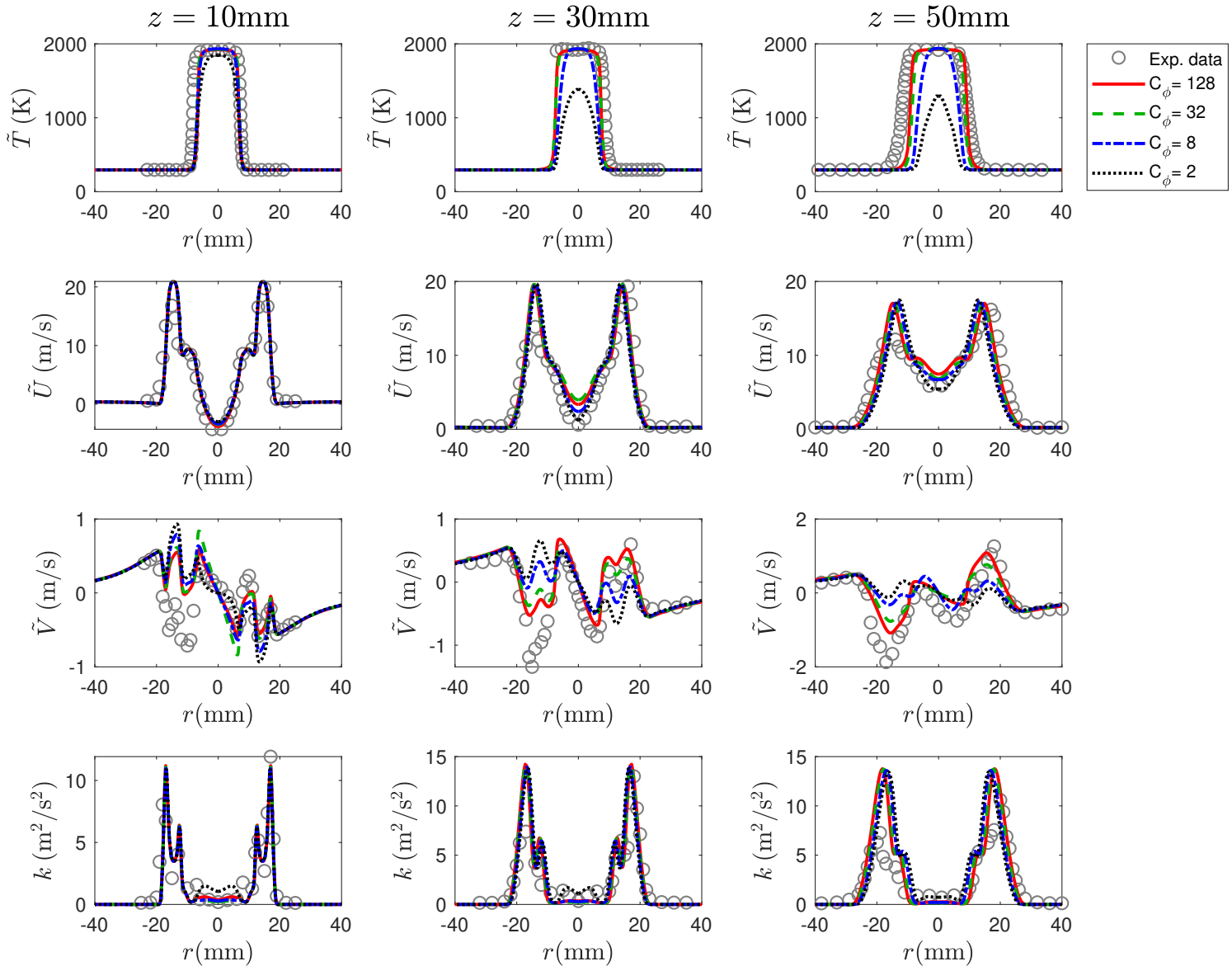

Figure 5.12. Effect of reducing the value of the mixing constant, C_ϕ on SwB1. From top to bottom: Static Temperature, Axial Velocity, Radial Velocity, Turbulent Kinetic Energy.

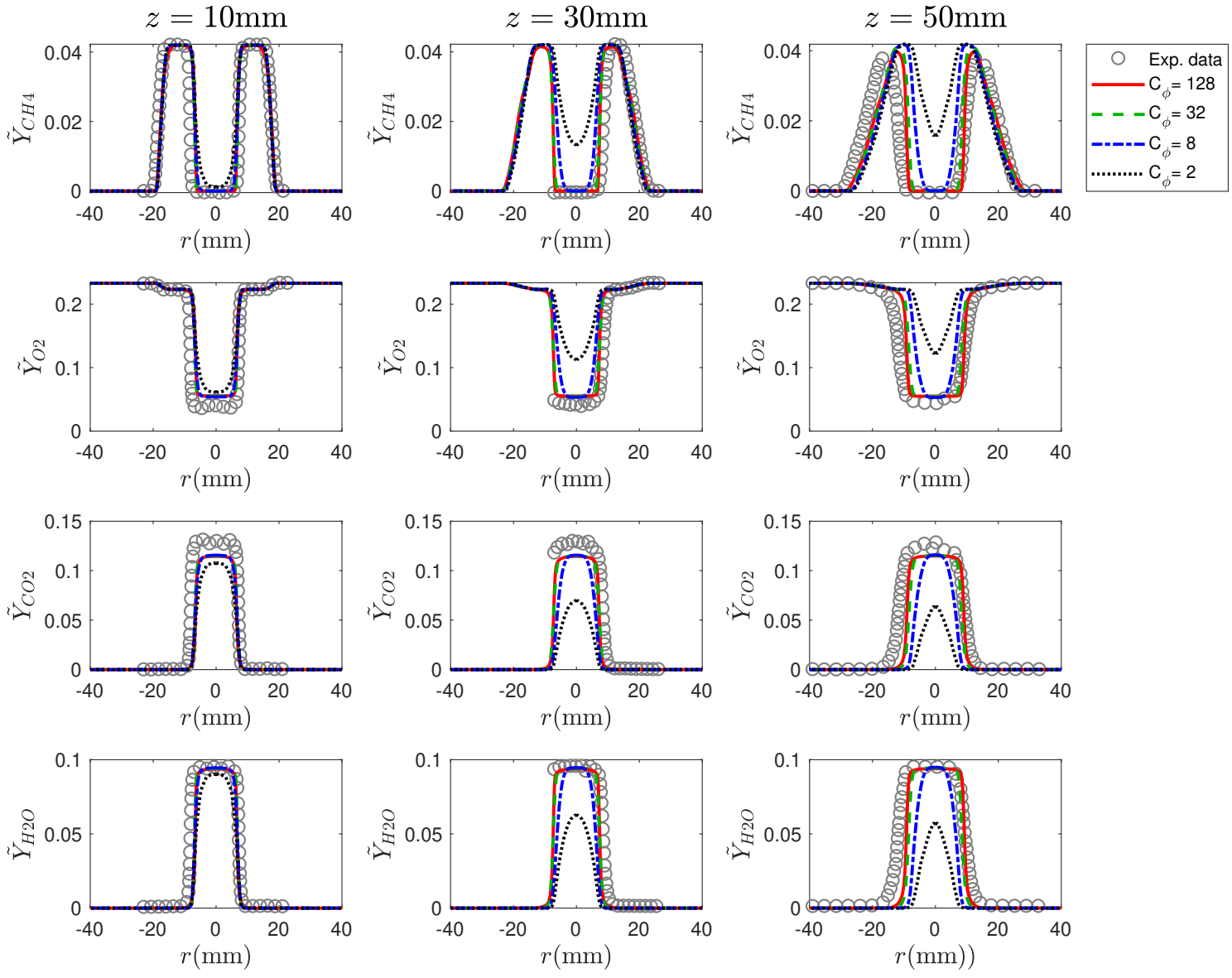

Figure 5.13. Effect of reducing the value of the mixing constant, C_ϕ on SwB1. From top to bottom: Mean mass fractions of CH_4, O_2, CO_2, and H_2O.

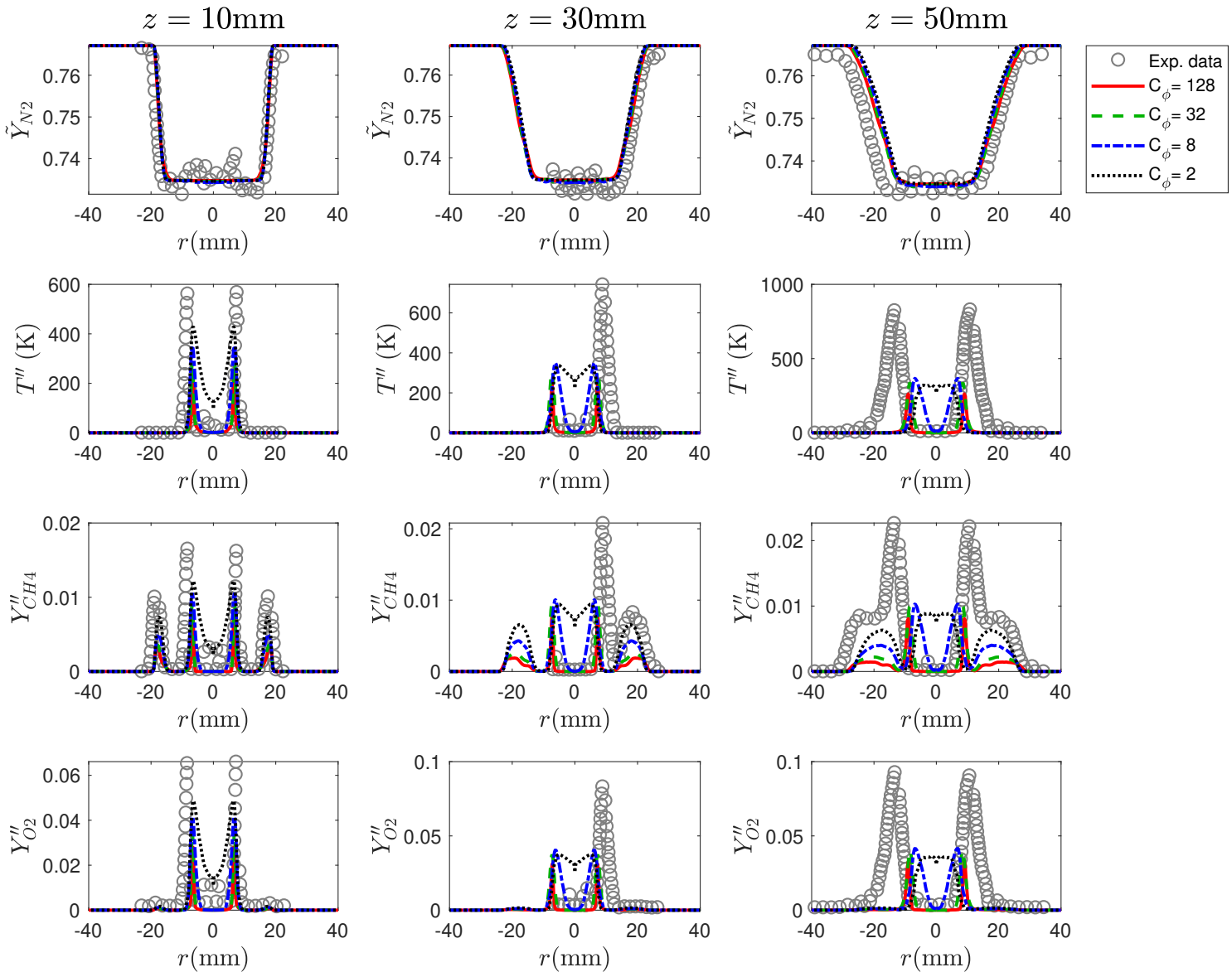

Figure 5.14. Effect of reducing the value of the mixing constant, C_ϕ on SwB1. From top to bottom: Mean mass fraction of N_2, RMS Temperature, RMS mass fractions of CH_4, and O_2.

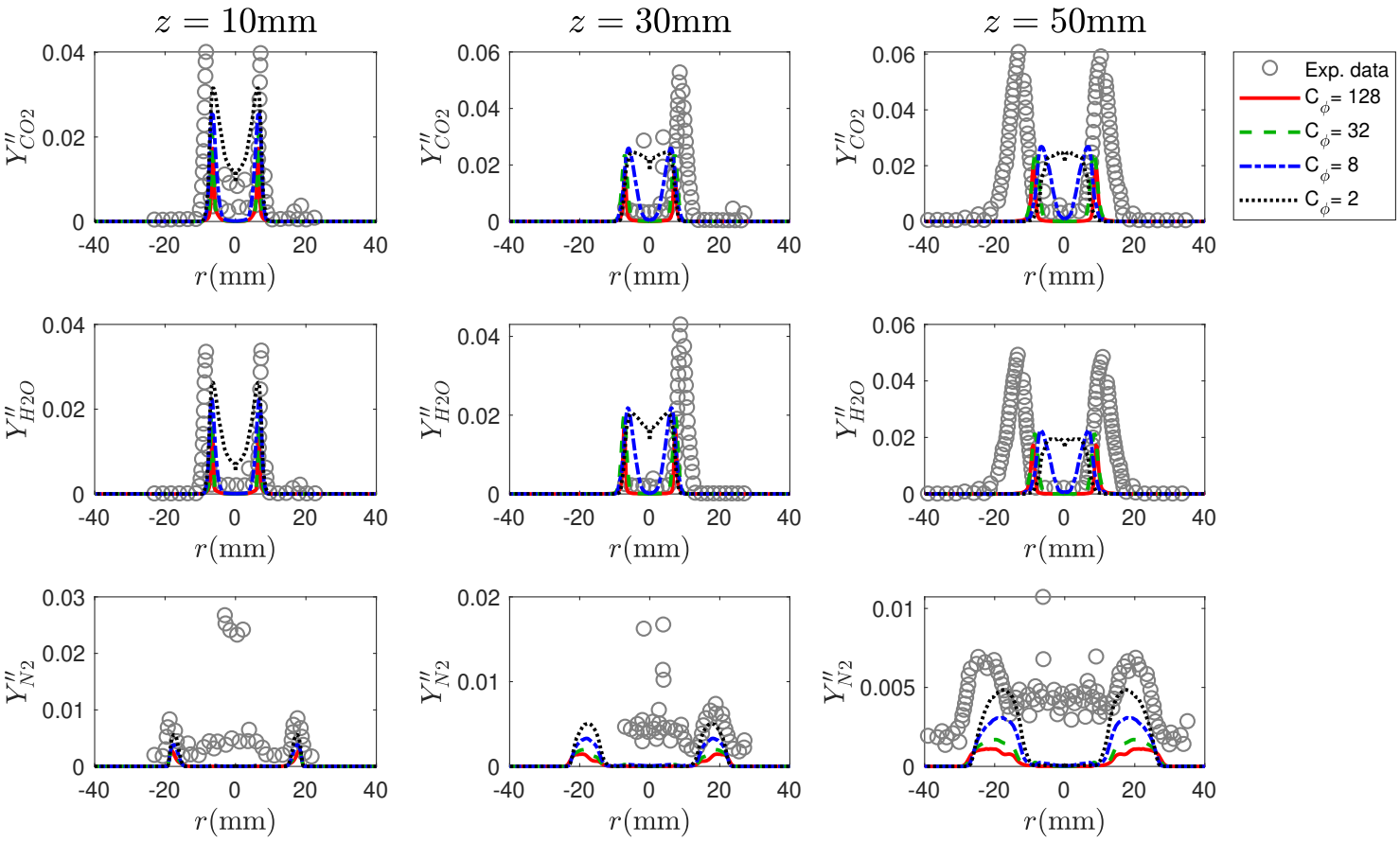

Figure 5.15. Effect of reducing the value of the mixing constant, C_ϕ on SwB1. From top to bottom: RMS mass fractions of CO_2, H_2O, and N_2.

5.6 Comparison of different mixing models

As mentioned earlier, FLUENT has multiple inbuilt mixing models. We have tried the IEM model and the Mcurl model to compare and see if either model works better for the case. The Figures 5.16, 5.17 and ref5.18 show plots of various quantities at different locations. It is observed that both the models overall perform quite similarly to each other and it is difficult to choose one over the other. The scalar fluctuations are underpredicted by both the models leading us to investigate further.

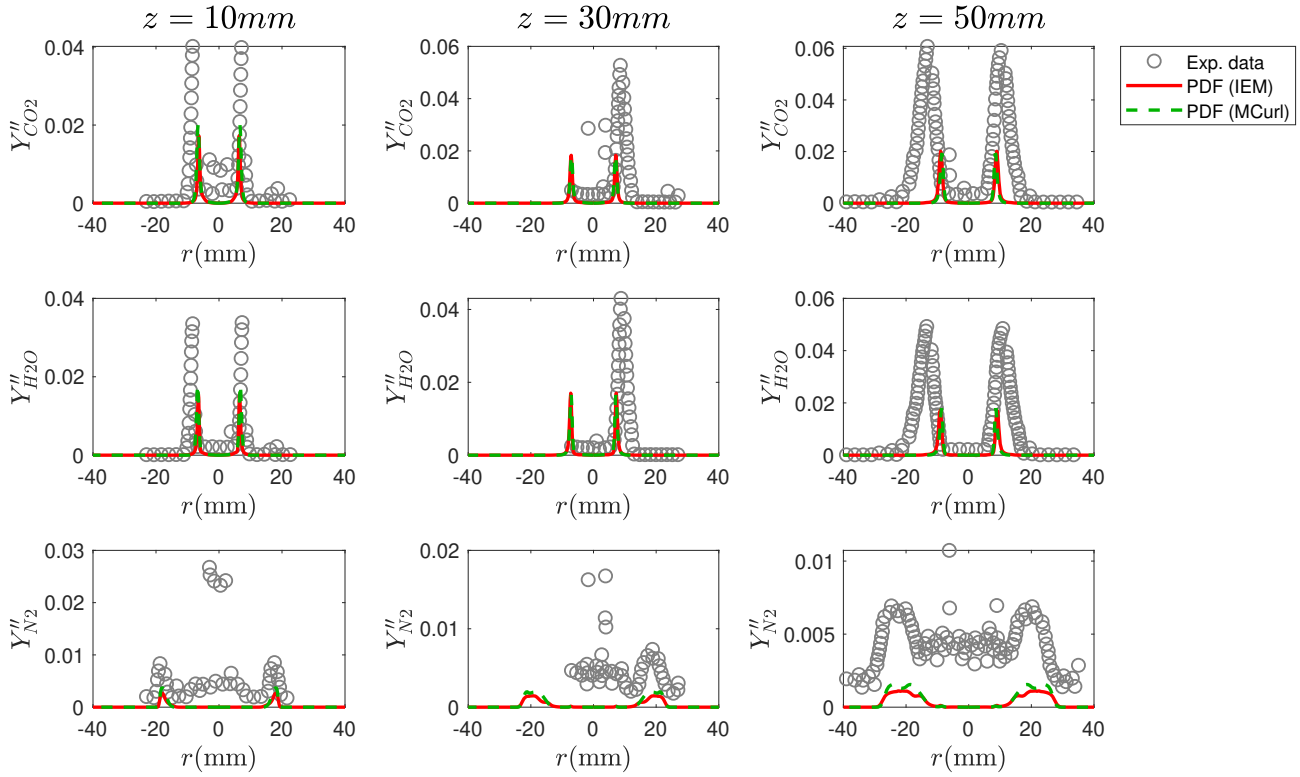

Figure 5.16. PDF transport method with IEM and MCurl mixing models on SwB1. From top to bottom: RMS mass fractions of CO_2, H_2O, and N_2.

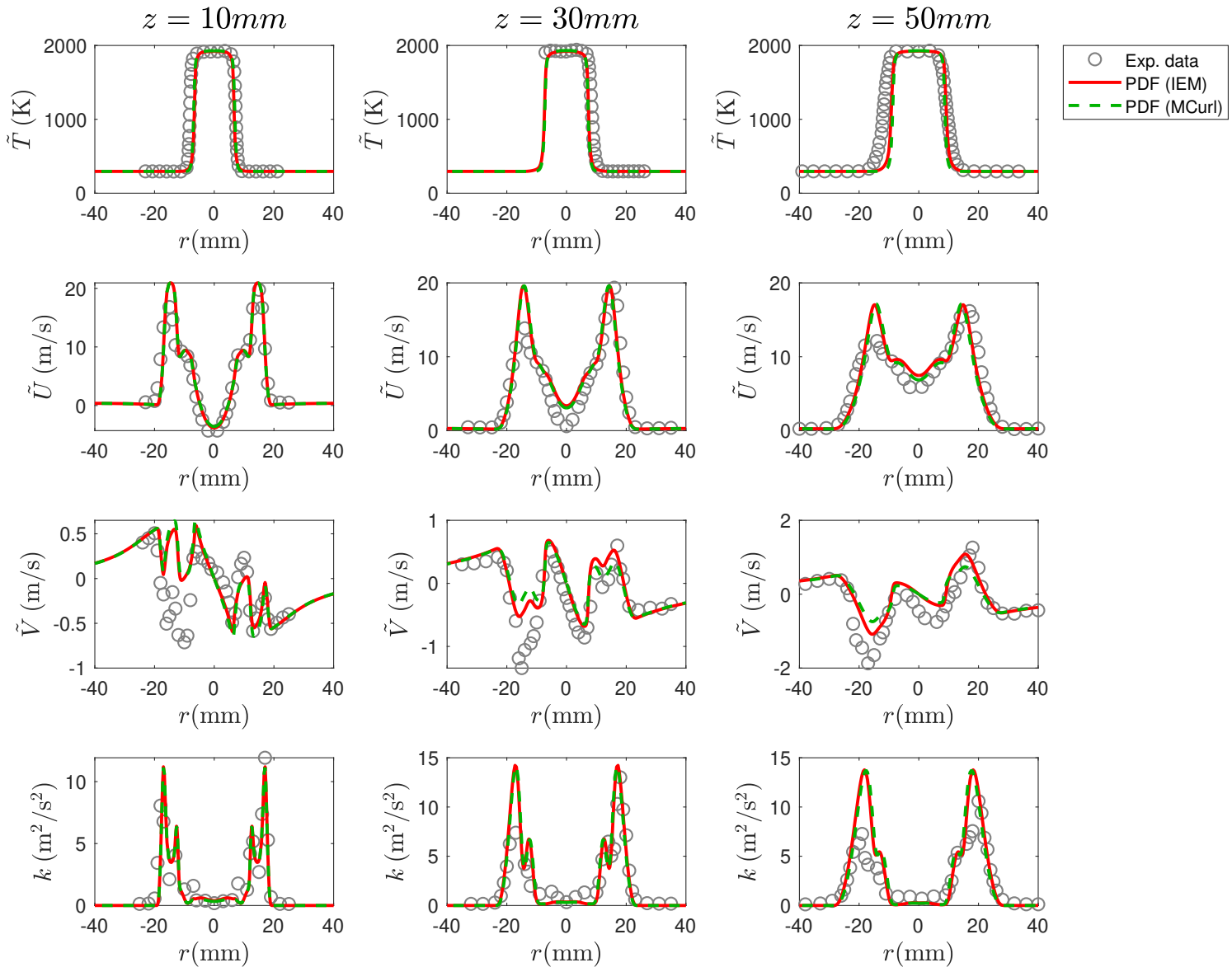

Figure 5.17. PDF transport method with IEM and MCurl mixing models on SwB1. From top to bottom: Static Temperature, Axial Velocity, Radial Velocity, turbulent kinetic energy.

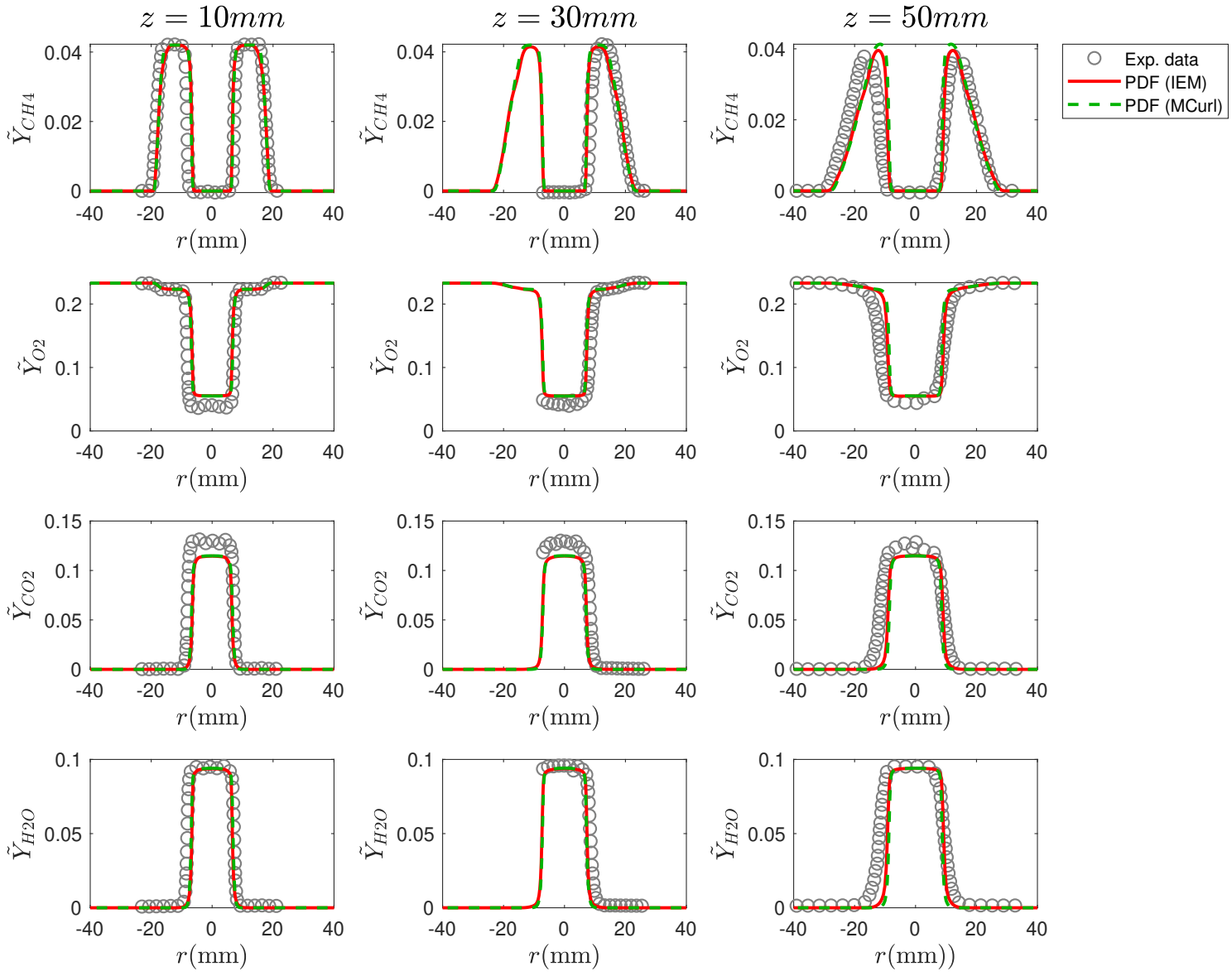

Figure 5.18. PDF transport method with IEM and MCurl mixing models on SwB1. From top to bottom: Mean mass fractions of CH_4, O_2, CO_2, and H_2O.

5.7 Implemented mixing models (Kuan et al. [27] and Kuran et al. [28])

As observed, while all the previous methods provided some insights or improvements to the results from the baseline case, there is still a large scope for improvement, especially with the scalar fluctuation results. As mentioned earlier, mixing has a fairly large role to play in the prediction of the rms values and hence two new mixing models were implemented using UDFs on FLUENT, the mathematical details of which are mentioned in the previous chapter.

If we look closely at the plots in Figure 5.19 and 5.20, we can see that both the models are able to capture all the mean scalars pretty well along with the high C_ϕ IEM model while the low C_ϕ case does not predict the means well. Looking at the scalar rms plots in Figure 5.21 and 5.22, we can see that the model by Kuan et al. [27] performs much better away from the axis while providing slightly better prediction close to the axis at all 3 axial locations. A point to note is that the near axis velocity was captured very well by the low C_ϕ IEM model which suggests that mixing may have a larger role to play than initially anticipated and hence requires further studies. We did not have time to look more into this so we decided to extend the models which work best for the SwB1 to the stratified cases.

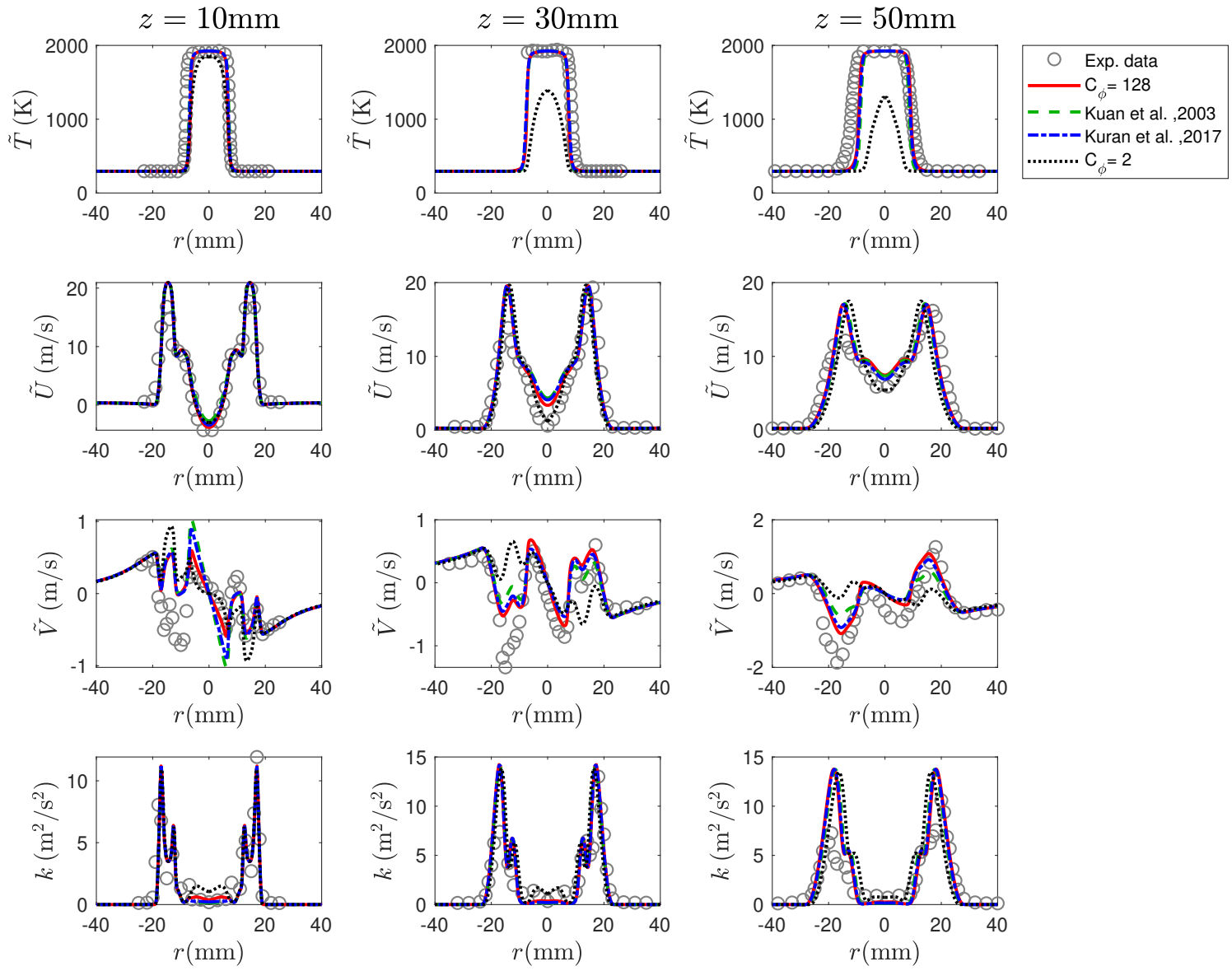

Figure 5.19. PDF IEM model with $C_\phi = 128$ and $C_\phi = 2$ compared with two mixing models defined in literature on SwB1. From top to bottom: Static Temperature, Axial Velocity, Radial Velocity, turbulent kinetic energy.

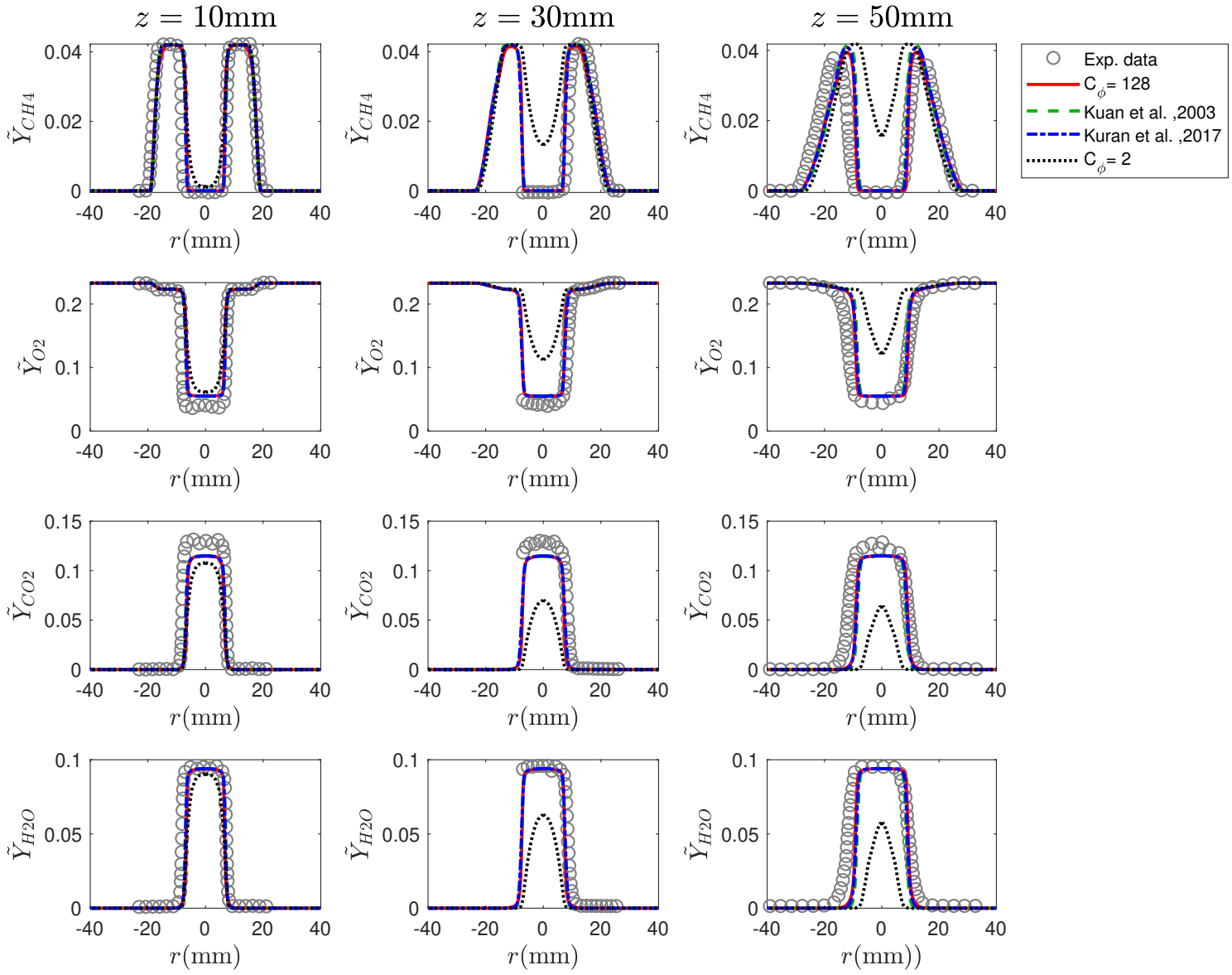

Figure 5.20. PDF IEM model with $C_\phi = 128$ and $C_\phi = 2$ compared with two mixing models defined in literature on SwB1. From top to bottom: Mean mass fractions of CH_4, O_2, CO_2, and H_2O.

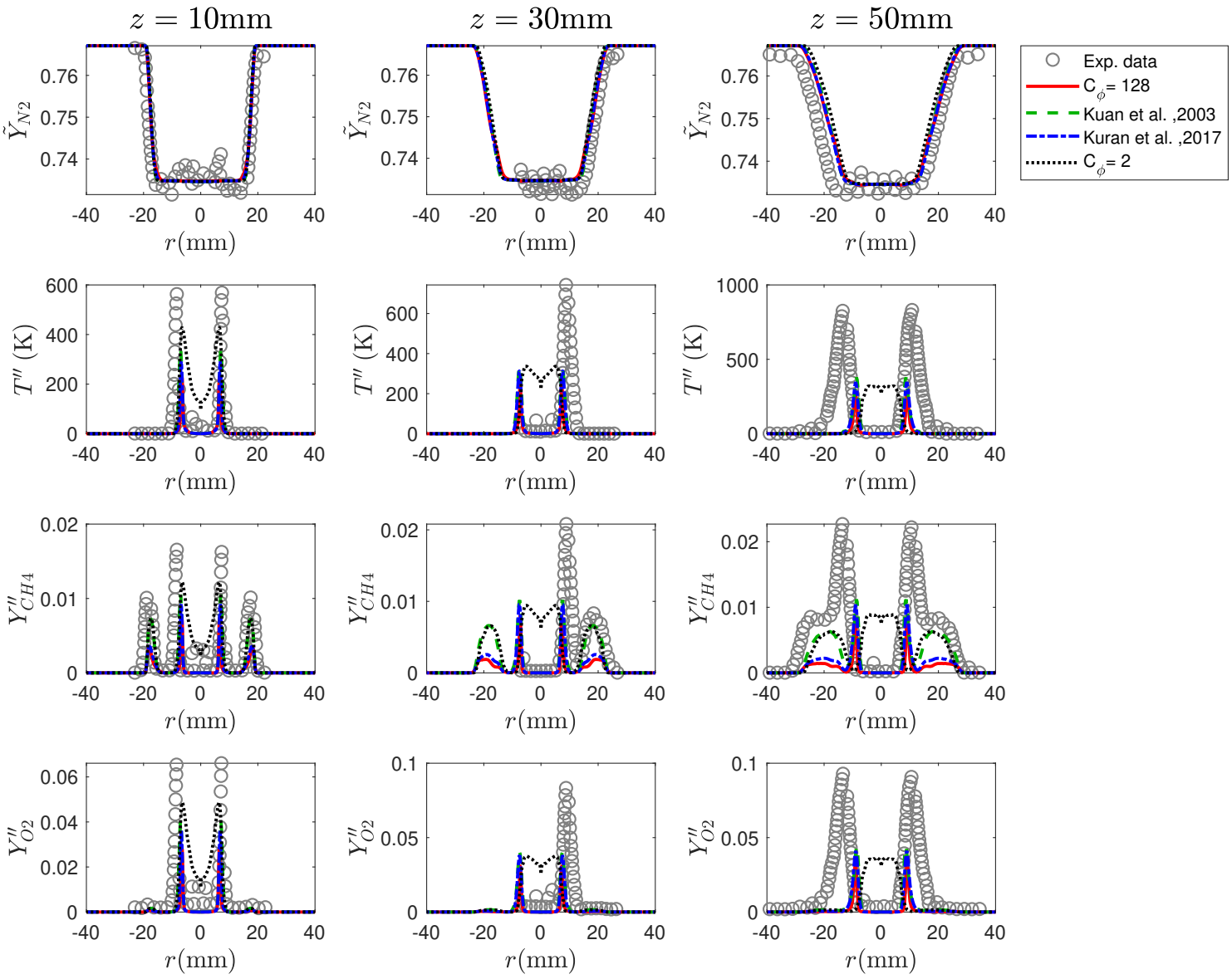

Figure 5.21. PDF IEM model with $C_\phi = 128$ and $C_\phi = 2$ compared with two mixing models defined in literature on SwB1. From top to bottom: Mean mass fraction of N_2, RMS Temperature, RMS mass fractions of CH_4, and O_2.

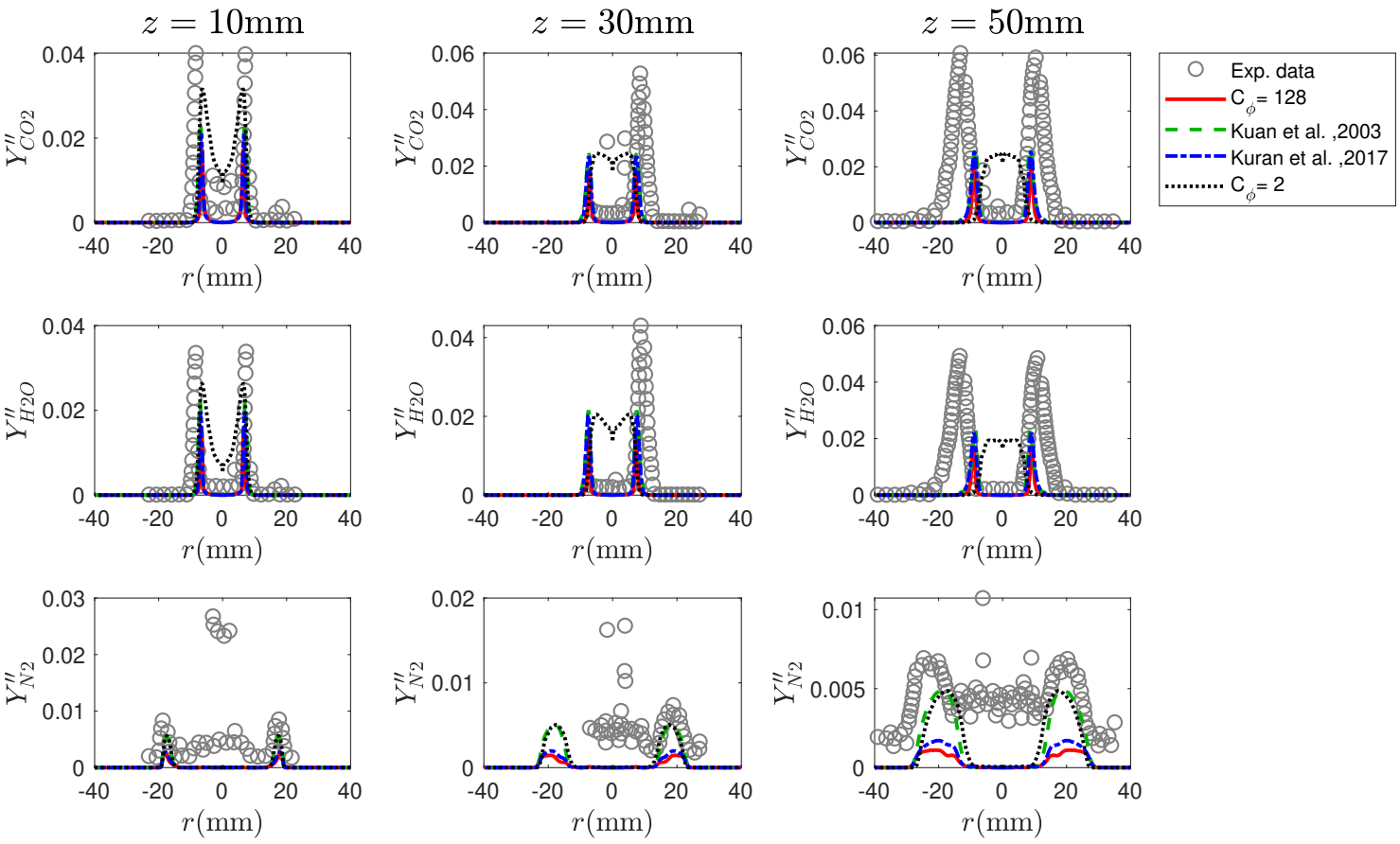

Figure 5.22. PDF IEM model with $C_\phi = 128$ and $C_\phi = 2$ compared with two mixing models defined in literature on SwB1. From top to bottom: RMS mass fractions of CO_2, H_2O, and N_2.

5.8 Results for SwB1

This section includes the final results for the non-stratified, premixed case. Observing the results, we can see that there is significant improvement from the baseline results. The fluctuation values are still under-predicted as seen in Figure 5.25 and 5.26 and further studies are required to identify and solve the issues. The mean scalar fields, as shown in Figure5.24, are captured quite well which is promising step. The velocity and turbulent kinetic energy are shown in Figure 5.23.

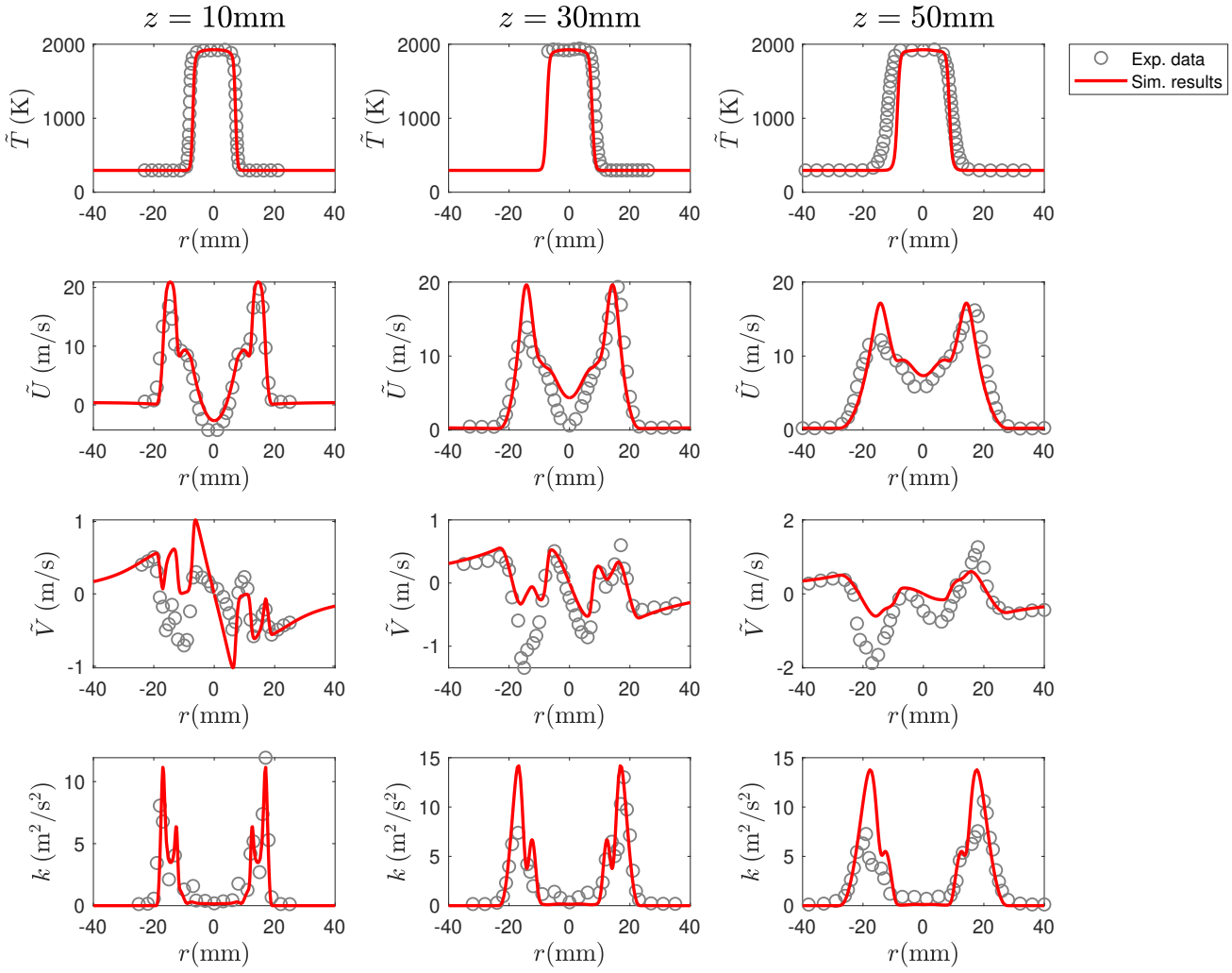

Figure 5.23. Results of PDF transport model with mixing model by Kuan et al. [27], Reynolds stress turbulence model on premixed conditions, SwB1. From top to bottom: Static Temperature, Axial Velocity, Radial Velocity, turbulent kinetic energy.

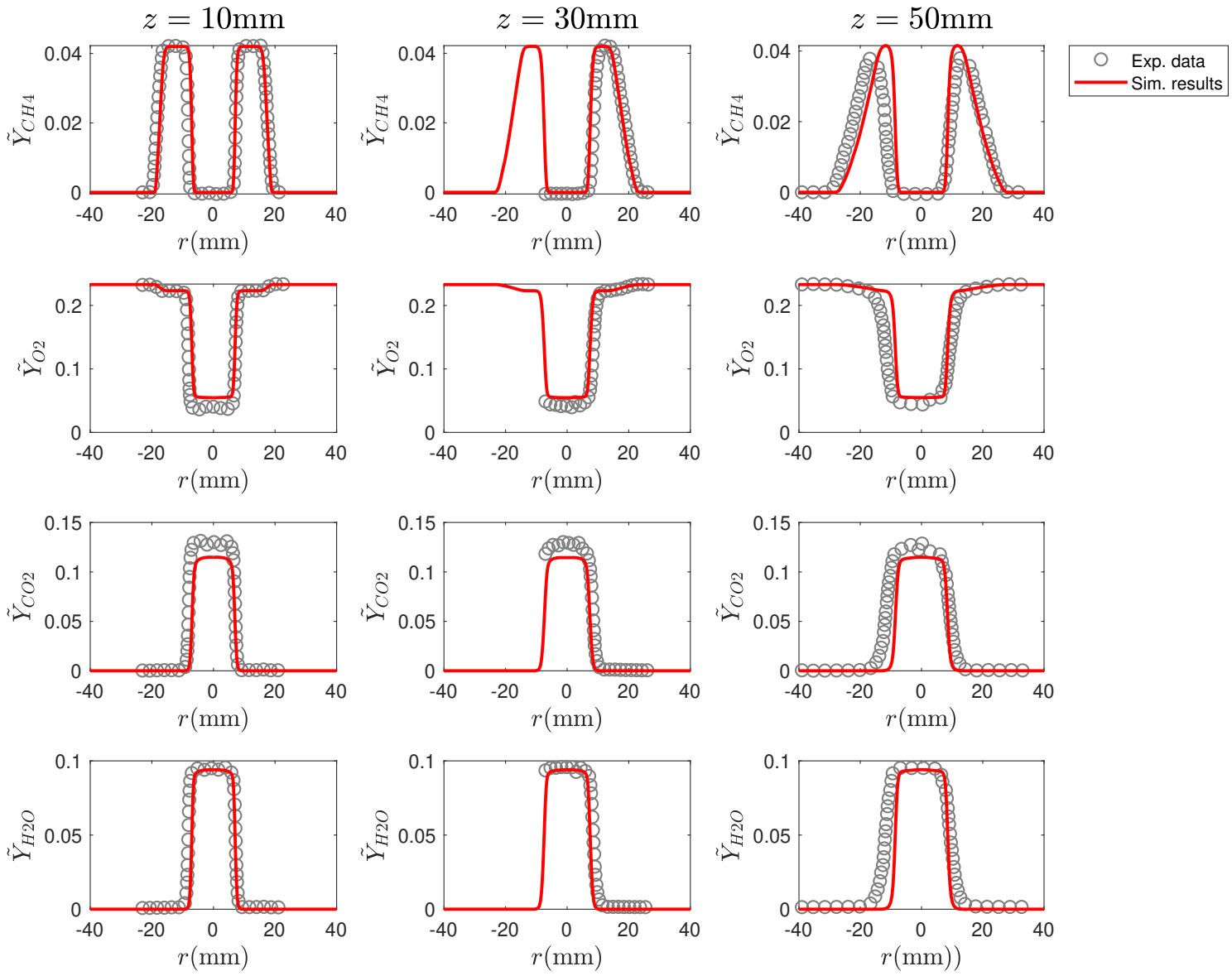

Figure 5.24. Results of PDF transport model with mixing model by Kuan et al. [27], Reynolds stress turbulence model on premixed conditions, SwB1. From top to bottom: Mean mass fractions of CH_4, O_2, CO_2, and H_2O.

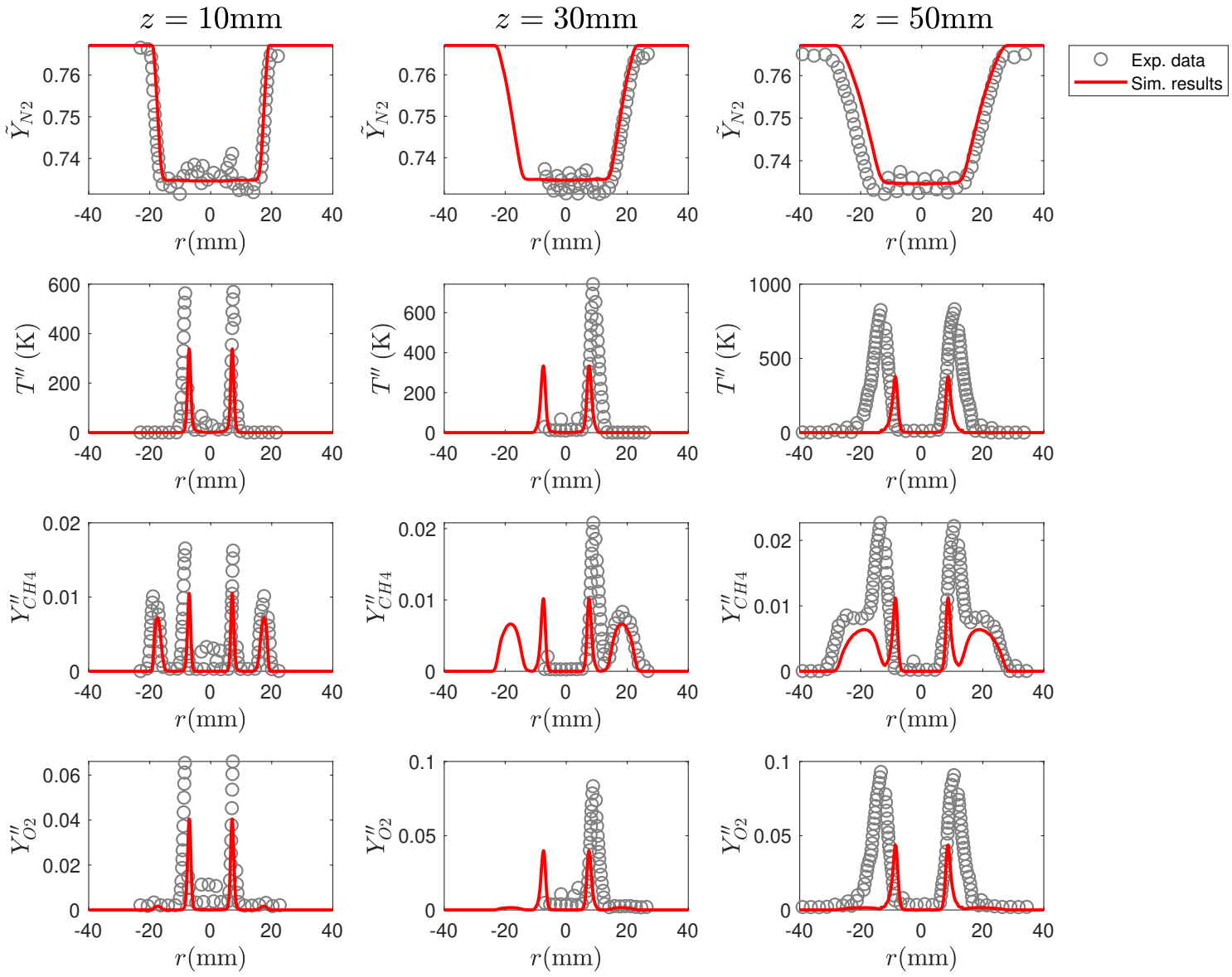

Figure 5.25. Results of PDF transport model with mixing model by Kuan et al. [27], Reynolds stress turbulence model on premixed conditions, SwB1. From top to bottom: Mean mass fraction of N_2, RMS Temperature, RMS mass fractions of CH_4, and O_2.

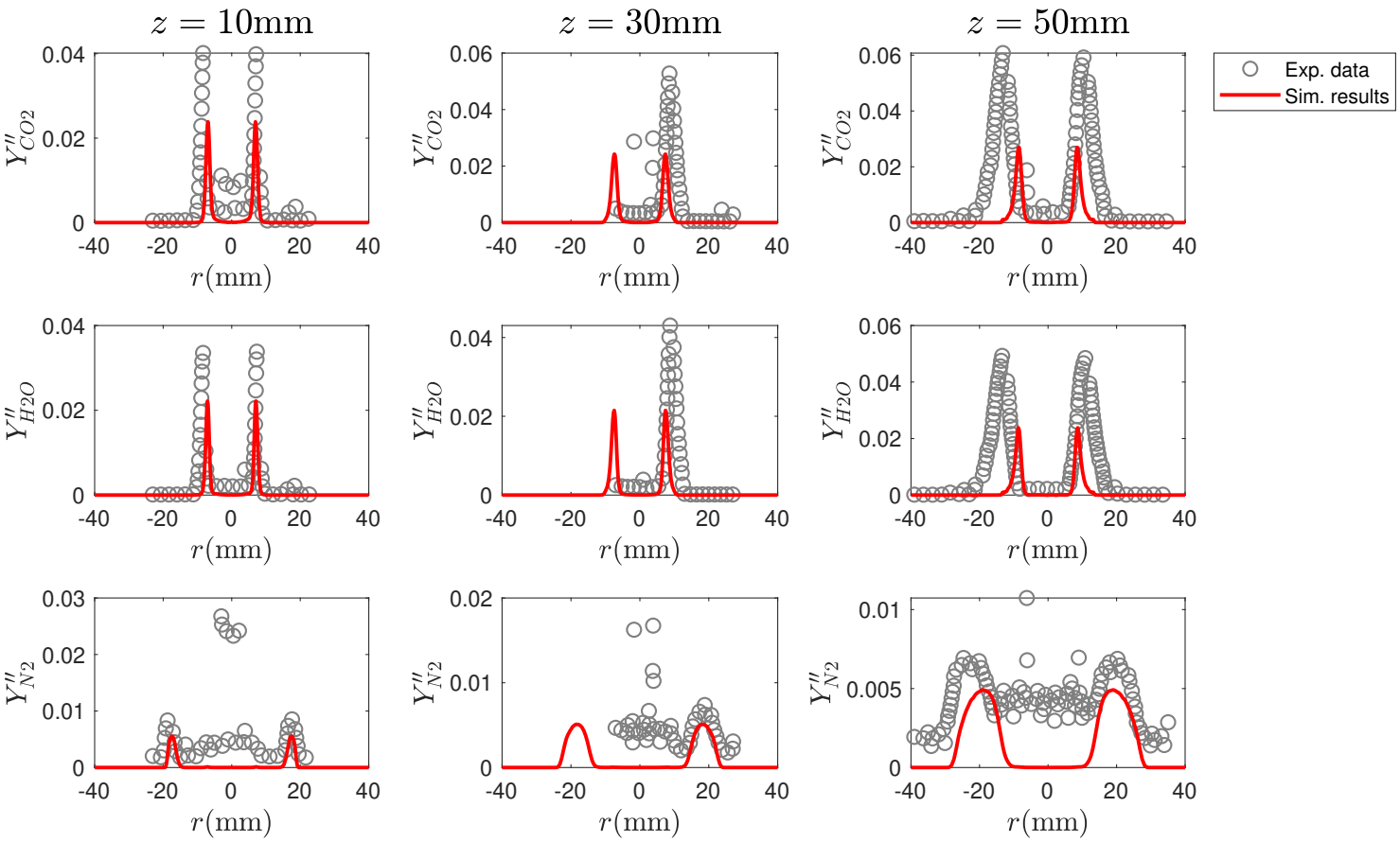

Figure 5.26. Results of PDF transport model with mixing model by Kuan et al. [27], Reynolds stress turbulence model on premixed conditions, SwB1. From top to bottom: RMS mass fractions of CO_2, H_2O, and N_2.

5.9 Results for SwB5

This section includes the results obtained for the moderately stratified case. The same grid, RSM turbulence model, transported PDF method with the mixing model by Kuan et al. [27] used for the premixed case are extended to simulate this case. The results show that the models perform well for stratified cases. The velocity (Figure 5.27) is captured much better near the axis and the scalar means (Figure 5.28) are predicted well in agreement with the experimental values. Although slightly under predicted near the axis and over predicted away from the axis, the turbulent kinetic energy is captured quite well qualitatively. The mean CH_4 values over shoot the expected values at downstream locations. The RMS values (Figure 5.29 and 5.30) are still under predicted and as mentioned earlier, need further investigation.

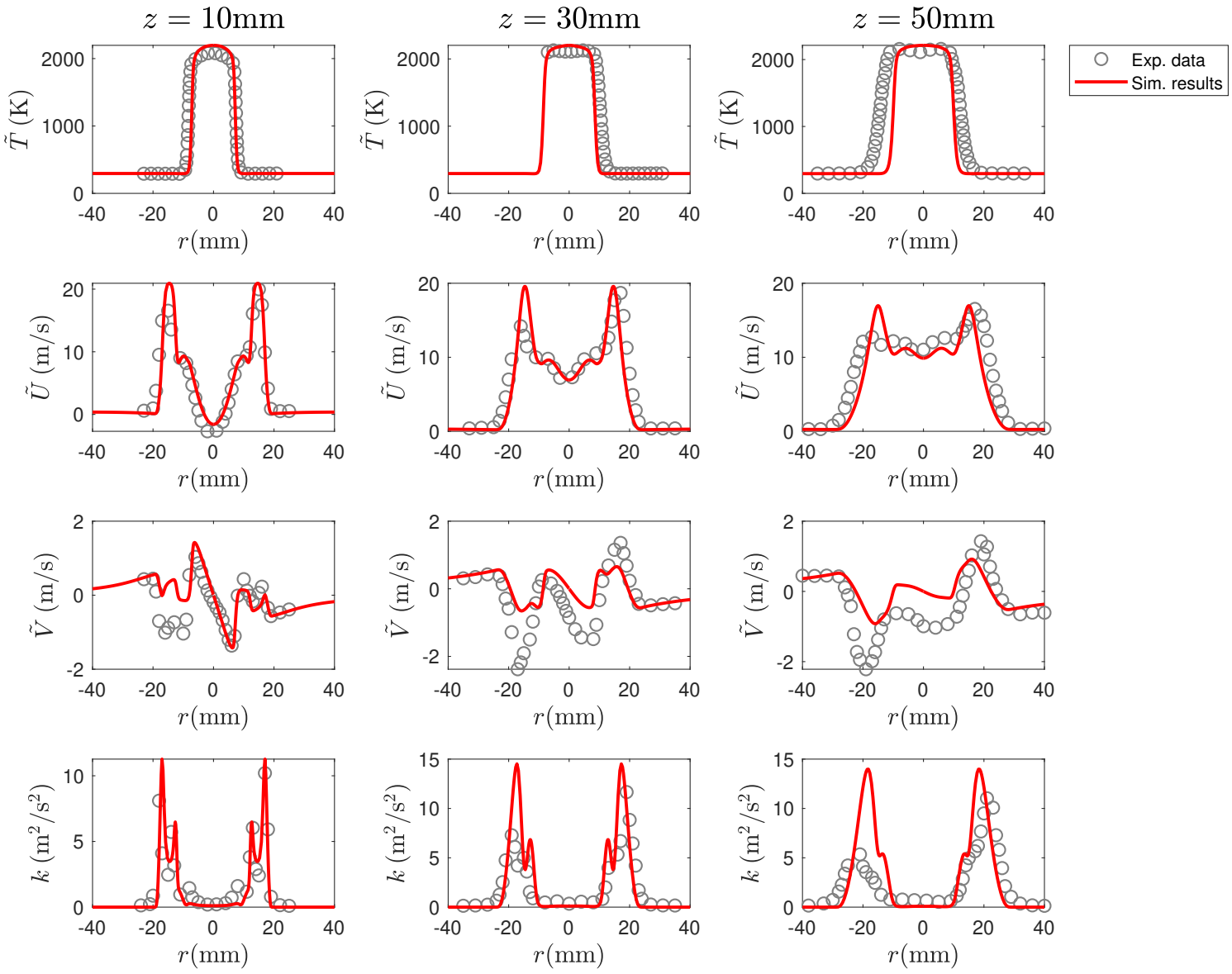

Figure 5.27. Results of PDF transport model with mixing model by Kuan et al. [27], Reynolds stress turbulence model on moderately stratified conditions, SwB5. From top to bottom: Static Temperature, Axial Velocity, Radial Velocity, turbulent kinetic energy.

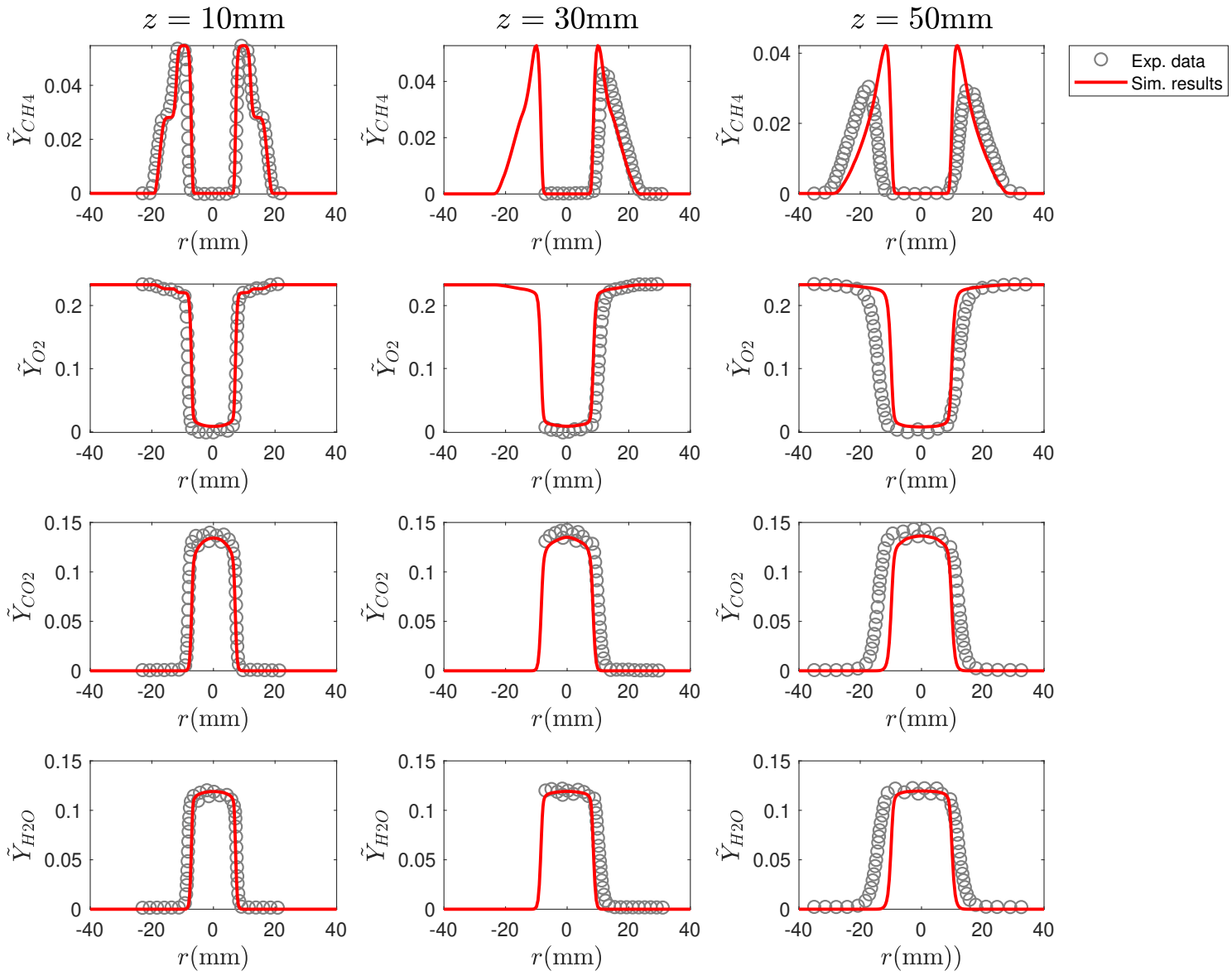

Figure 5.28. Results of PDF transport model with mixing model by Kuan et al. [27], Reynolds stress turbulence model on moderately stratified conditions, SwB5. From top to bottom: Mean mass fractions of CH_4, O_2, CO_2, and H_2O.

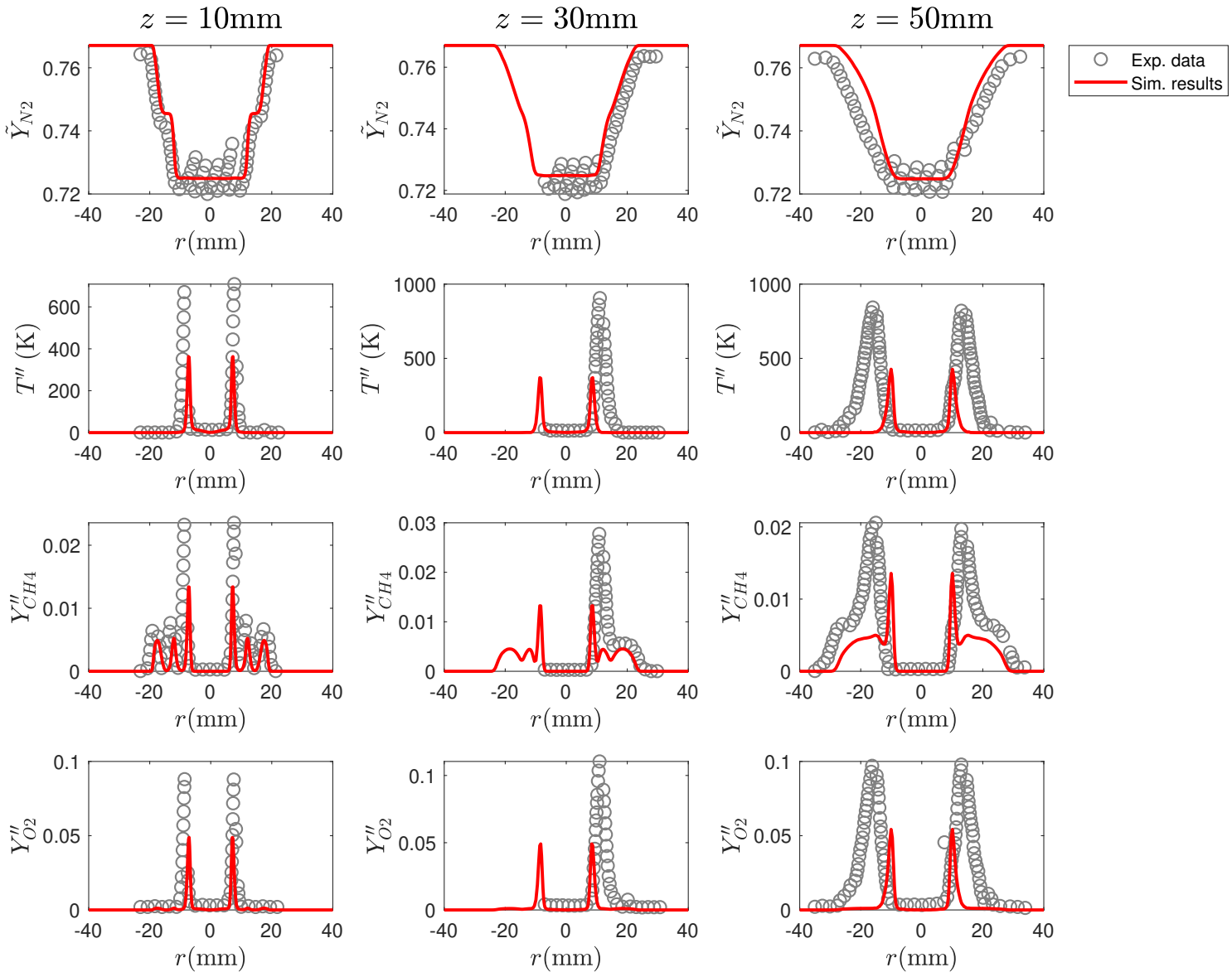

Figure 5.29. Results of PDF transport model with mixing model by Kuan et al. [27], Reynolds stress turbulence model on moderately stratified conditions, SwB5. From top to bottom: Mean mass fraction of N_2, RMS Temperature, RMS mass fractions of CH_4, and O_2.

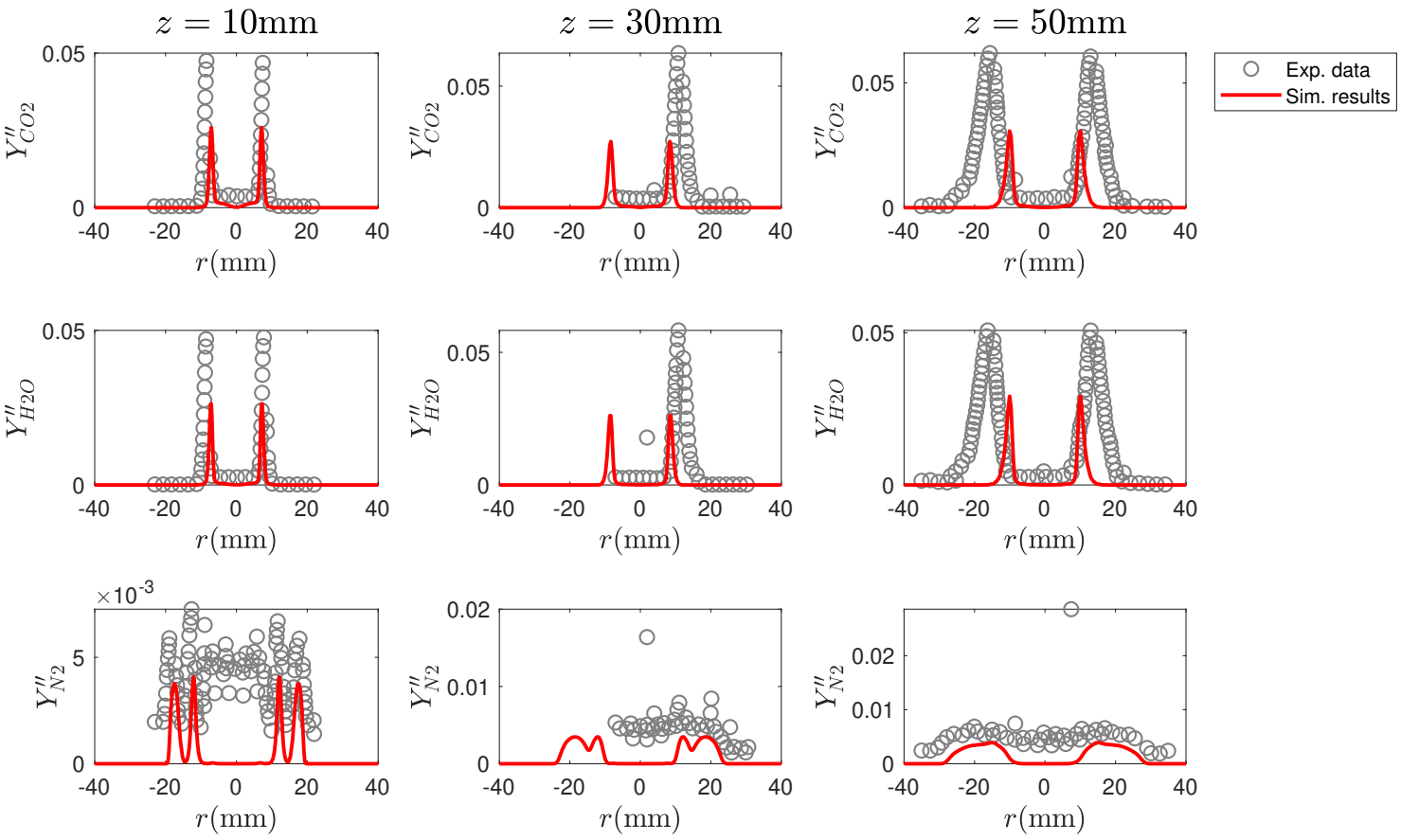

Figure 5.30. Results of PDF transport model with mixing model by Kuan et al. [27], Reynolds stress turbulence model on moderately stratified conditions, SwB5. From top to bottom: RMS mass fractions of CO_2, H_2O, and N_2.

5.10 Results for SwB9

This section includes the results obtained for the highly stratified case. Similar to SwB5, the models used for SwB1 were extended for this case and the premix composition was altered according to the case specifications. The models still perform for such high levels of stratification, the predicted values being very close to the experimental. This shows that the PDT method can capture stratified combustion accurately. Overprediction of CH_4 at $z = 30$mm and $z = 50$mm continues to persist. The under prediction of RMS values also extends on to high levels of stratification and requires further investigation. These results are shown in Figures 5.31, 5.32, 5.33, and 5.34.

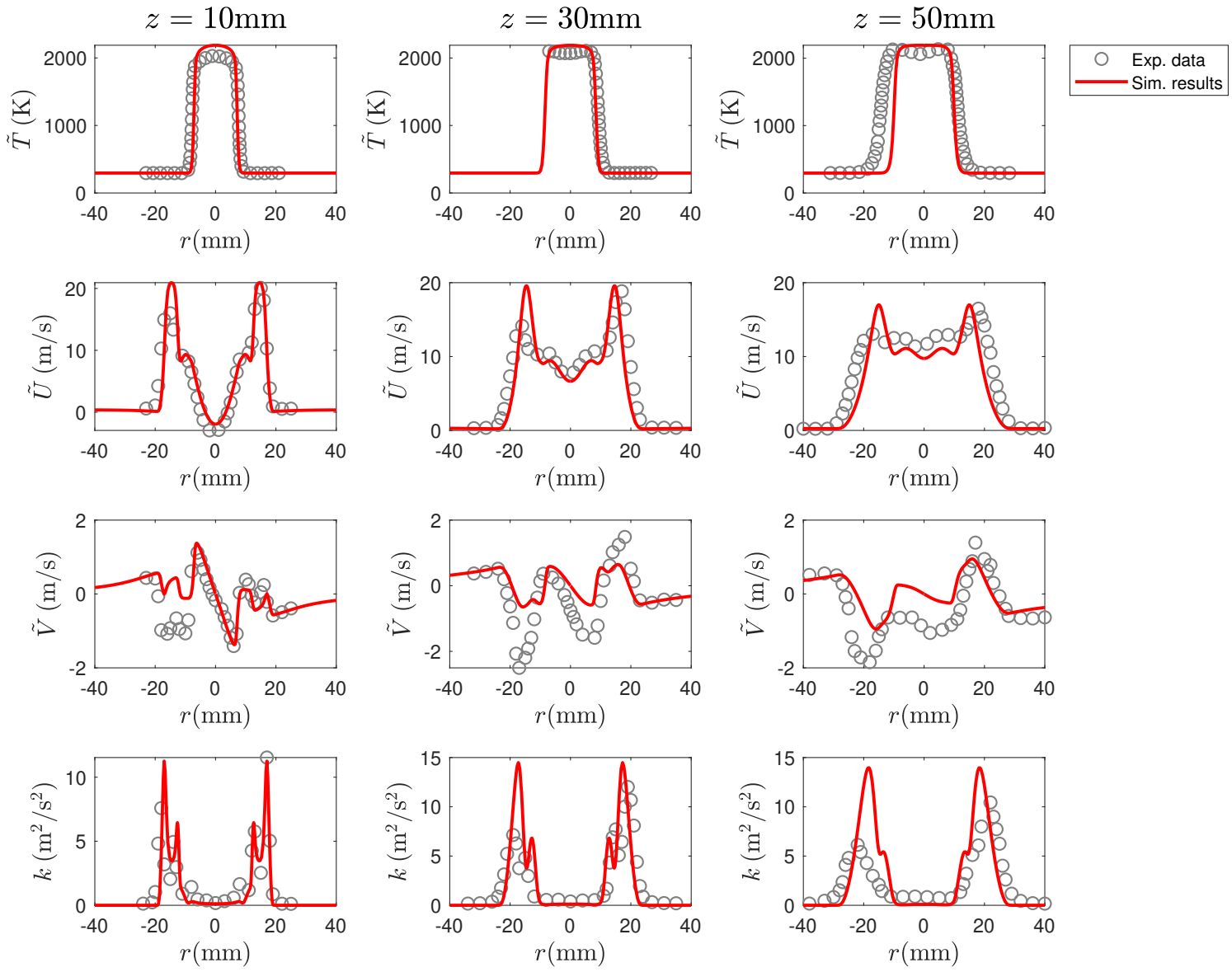

Figure 5.31. Results of PDF transport model with mixing model by Kuan et al. [27], Reynolds stress turbulence model on highly stratified conditions, SwB9. From top to bottom: Static Temperature, Axial Velocity, Radial Velocity, turbulent kinetic energy.

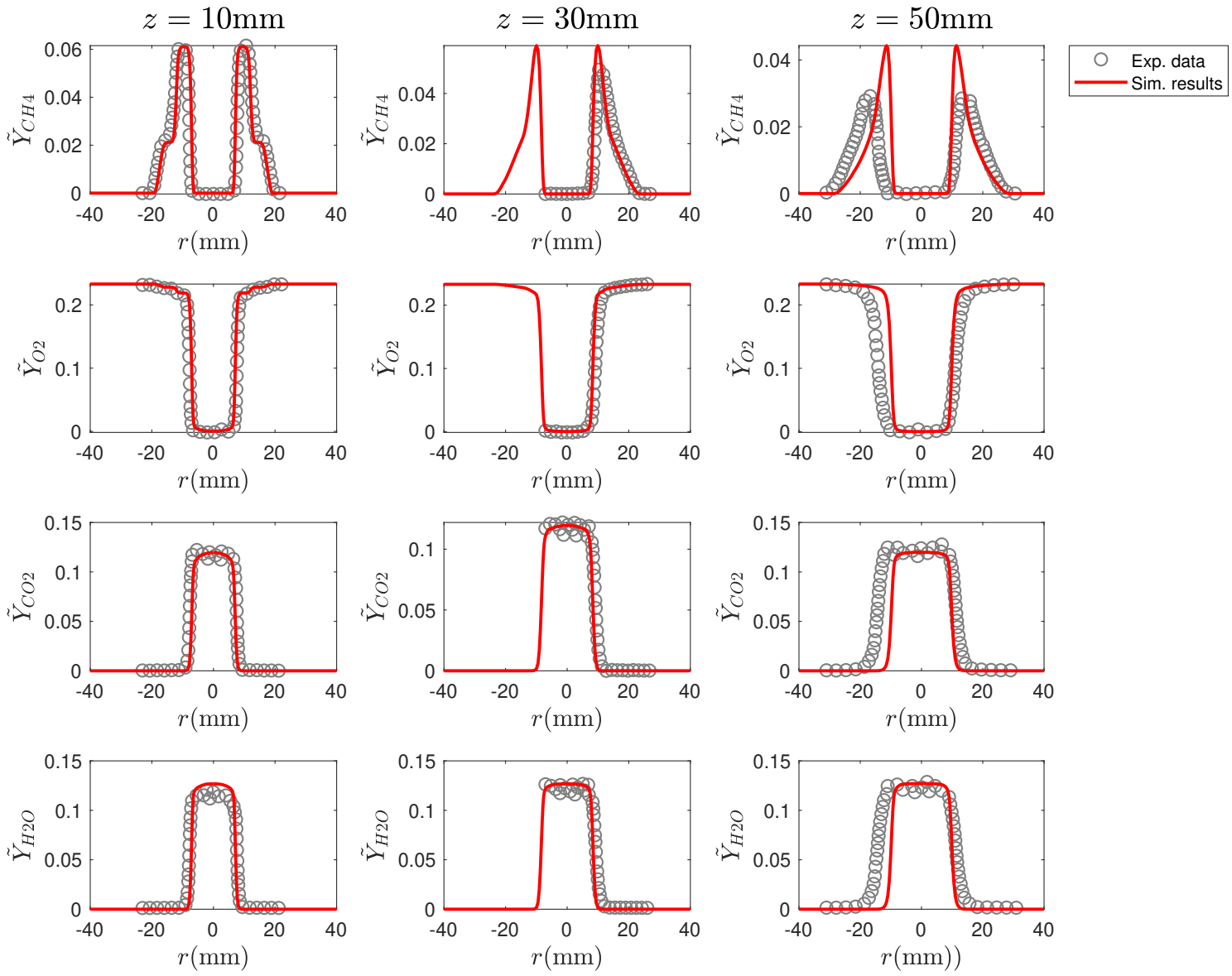

Figure 5.32. Results of PDF transport model with mixing model by Kuan et al. [27], Reynolds stress turbulence model on highly stratified conditions, SwB9. From top to bottom: Mean mass fractions of CH_4, O_2, CO_2, and H_2O.

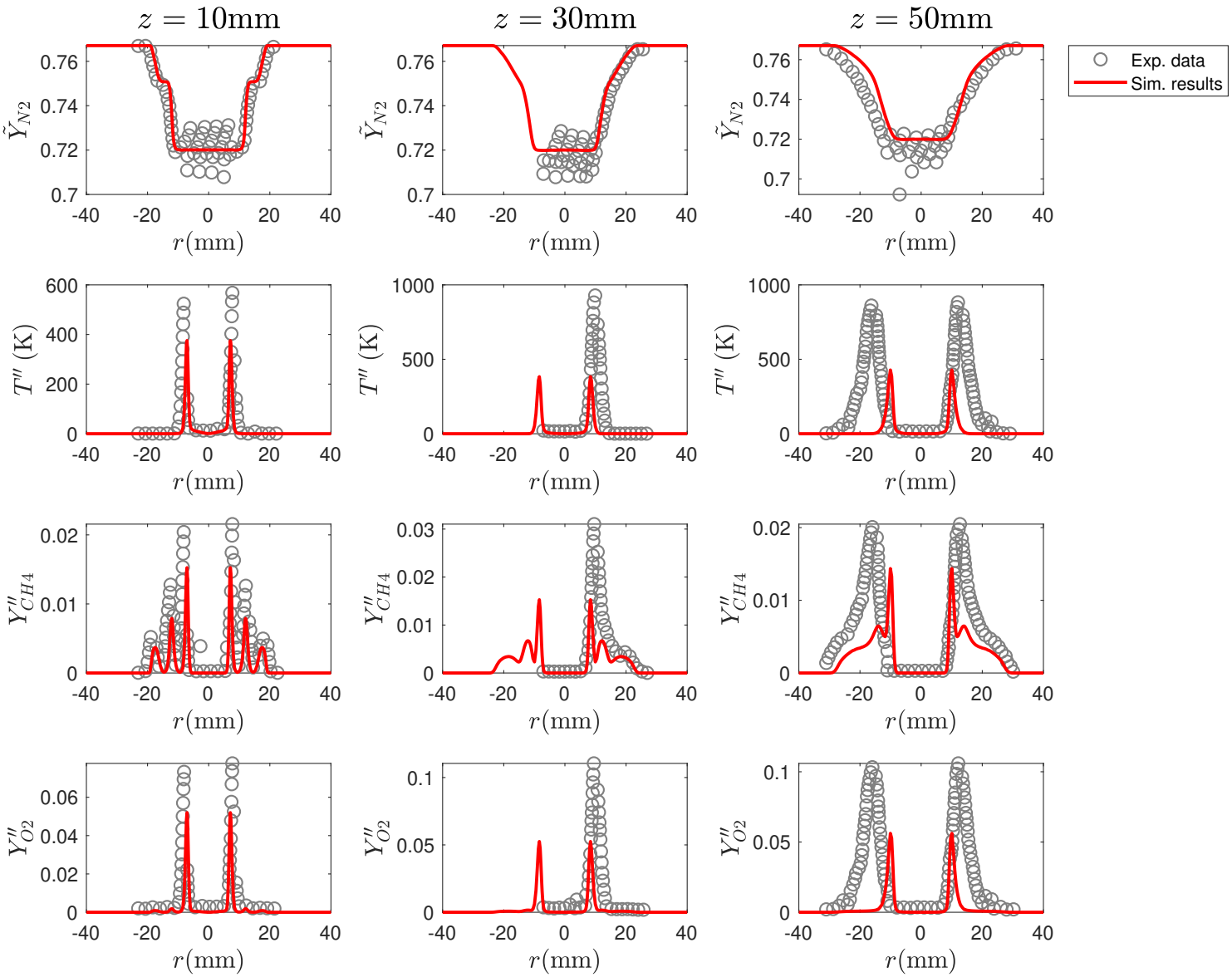

Figure 5.33. Results of PDF transport model with mixing model by Kuan et al. [27], Reynolds stress turbulence model on highly stratified conditions, SwB9. From top to bottom: Mean mass fraction of N_2, RMS Temperature, RMS mass fractions of CH_4, and O_2.

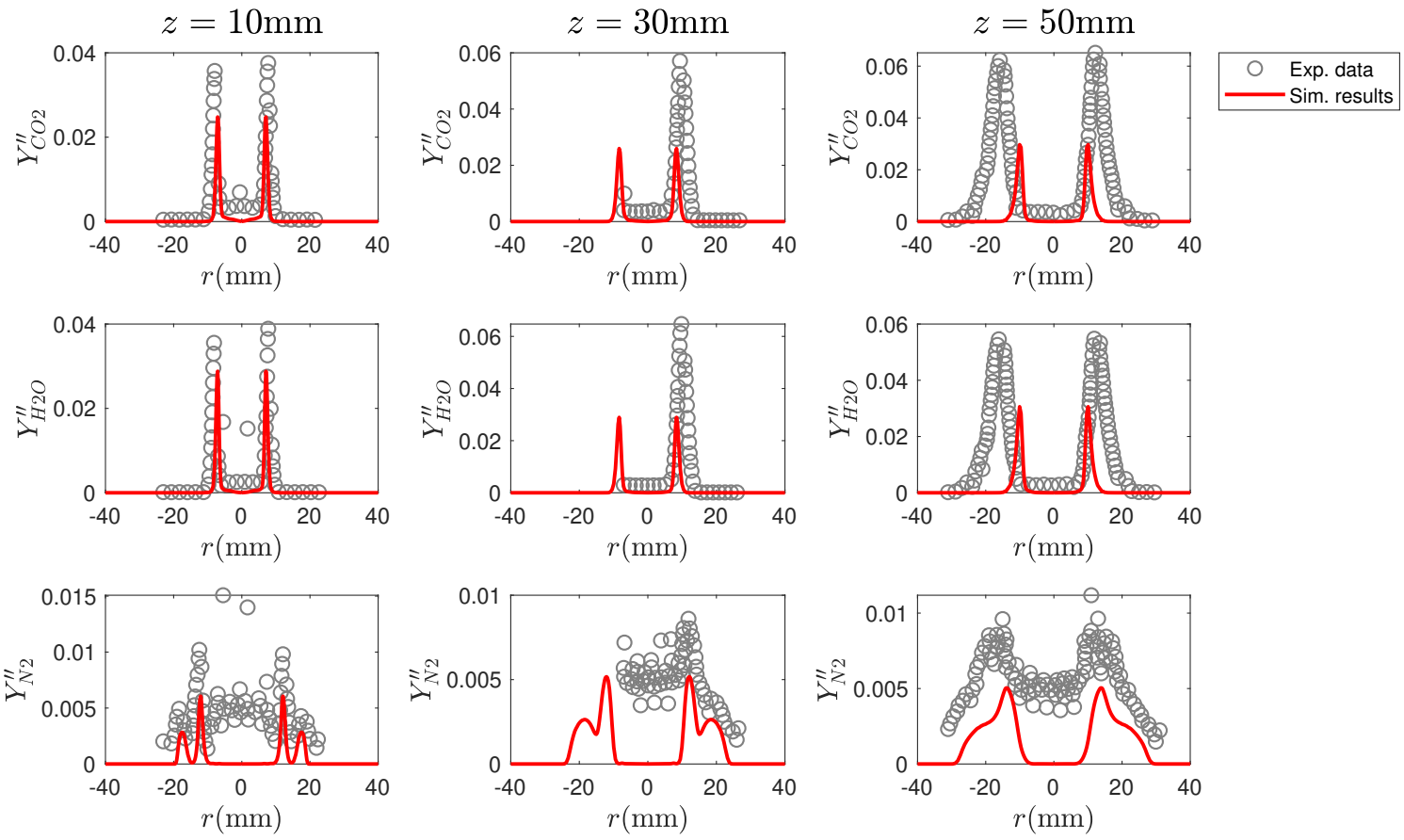

Figure 5.34. Results of PDF transport model with mixing model by Kuan et al. [27], Reynolds stress turbulence model on highly stratified conditions, SwB9. From top to bottom: RMS mass fractions of CO_2, H_2O, and N_2.

6. CONCLUSIONS AND FUTURE WORK

The numerical study of the Cambridge Stratified burner leads us to a few significant conclusions. We can observe that the transported PDF model can capture the major features of the reacting cases considered in this study with reasonable accuracy. It is suitable for predicting homogeneous premixed flames as well as stratified flames. Although more computationally expensive, the Reynolds Stress model is a good fit with the transported PDF method for modeling turbulence in stratified flames. The velocity field is captured well, but the turbulent kinetic energy is slightly overpredicted away from the axis at downstream locations outside the recirculation zone. The importance of accurately modeling mixing is made clear in the results. For the IEM model, setting a high mixing constant value seems to provide a good match with the experimental values for mean scalars but underpredicts the scalar fluctuations. Low mixing constant value simulations underpredict the overall scalar field and fail to capture the qualitative features. This study also leads to the conclusion that two-dimensional RANS modeling, is capable of predicting the results of stratified combustion with good accuracy. The stratified cases have a similar trend in the accuracy of predictions as the premixed case, which shows that the models can be extended well to capture stratified flames. One issue specific to the stratified cases is the overprediction of mean CH_4 at downstream locations.

Velocity fields are captured slightly better by the low mixing constant models, which gives rise to maybe developing a new mixing model keeping this in mind. Further work is required to understand the correlation between the mixing constant and velocity field and on developing models to capture both the scalar and near axis velocity fields accurately.

REFERENCES

[1] A. Sun, R. Adler, J. Berry, J. Michaels, S. G. Grape, R. Sommer, T. S. C. R. Namovicz, J. Barrick, M. K. amd Jennifer Wade, R. Berry, L. Cabral, T. Shear, L. Jamison, P. Lindstrom, and G. McGrath, "Annual energy review," *Technical report, U.S.Energy Information Administration*, 2011. [Online]. Available: https://www.eia.gov/totalenergy/data/annual/pdf/aer.pdf.

[2] "Fuels as sources of energy," *Thermopedia*, 2021. [Online]. Available: https://chem.libretexts.org/@go/page/6316.

[3] S. R. Turns *et al.*, *Introduction to combustion*, 1996.

[4] Williams.A, "Flames," *Thermopedia*, 2011.

[5] M. Day, S. Tachibana, J. Bell, M. Lijewski, V. Beckner, and R. K. Cheng, "A combined computational and experimental characterization of lean premixed turbulent low swirl laboratory flames: I. methane flames," *Combustion and Flame*, vol. 159, no. 1, pp. 275–290, 2012, ISSN: 0010-2180.

[6] "Nobert peters, lecture notes," 2010. [Online]. Available: https://cefrc.princeton.edu/sites/cefrc/files/Files/2010%20Lecture%20Notes/Norbert%20Peters/Lecture8.pdf.

[7] "Chapter 15 - combustion and flames," D. E. Winterbone and A. Turan, Eds., pp. 323–344, 2015.

[8] A. N. Lipatnikov, "Stratified turbulent flames: Recent advances in understanding the influence of mixture inhomogeneities on premixed combustion and modeling challenges," *Progress in Energy and Combustion Science*, vol. 62, pp. 87–132, 2017, ISSN: 0360-1285.

[9] H. Breitbach, A. Waltner, T. Landenfeld, and C. Schwarz, "Lean-burn stratified combustion at gasoline engines," *MTZ worldwide*, vol. 74, 2013, ISSN: 2192-9114.

[10] C. Karagiannaki, G. Paterakis, K. Souflas, E. Dogkas, and P. Koutmos, "Performance evaluation of a model swirl burner under premixed or stratified inlet mixture conditions," *Journal of Engineering Energy*, vol. 141, 2015.

[11] M. S. Sweeney, S. Hochgreb, M. J. Dunn, and R. S. Barlow, "The structure of turbulent stratified and premixed methane/air flames i: Non-swirling flows," *Combustion and Flame*, vol. 159, no. 9, pp. 2896–2911, 2012.

[12] S. Pope, "Pdf methods for turbulent reactive flows," *Progress in Energy and Combustion Science*, vol. 11, no. 2, pp. 119–192, 1985.

[13] "Ansys fluent user guide 2020 r1," 2020.

[14] F. Seffrin, F. Fuest, D. Geyer, and A. Dreizler, "Flow field studies of a new series of turbulent premixed stratified flames.," *Combustion and Flame*, vol. 157, 2010.

[15] V. Robin, A. Mura, M. Champion, O. Degardin, B. Renou, and A. Boukhalfa, "Experimental and numerical analysis of stratified turbulent v-shaped flames," *Combustion and Flame*, vol. 153, pp. 288–315, Apr. 2008.

[16] T. Brauner, W. P. Jones, and A. J. Marquis, "Les of the cambridge stratified swirl burner using a sub-grid pdf approach," *Flow, Turbulence and Combustion*, vol. 96, 2016.

[17] F. Proch and A. M. Kempf, "Numerical analysis of the cambridge stratified flame series using artificial thickened flame les with tabulated premixed flame chemistry," *Combustion and Flame*, vol. 161, 2014.

[18] R. Mercier, F. Proch, A. Kempf, and B. FIORINA, "Numerical and modeling strategies for the simulation of the cambridge stratified flame series," Jan. 2013.

[19] H. Zhang, T. Ye, G. Wang, P. Tang, and M. Liu, "Large eddy simulation of turbulent premixed swirling flames using dynamic thickened flame with tabulated detailed chemistry," *Flow, Turbulence and Combustion*, vol. 98, 2017.

[20] Y. Xiao, Z. Lai, and W. Song, "Large eddy simulation of premixed stratified swirling flame using the finite rate chemistry approach," *International Journal of Aerospace Engineering*, 2019.

[21] H. Turkeri, X. Zhaoa, S. B. Pope, and M. Muradogluc, "Large eddy simulation/probability density function simulations of the cambridge turbulent stratified flame series," *Combustion and Flame*, vol. 199, 2019.

[22] W. Zhang, S. Karaca, J. Wang, Z. Huang, and J. van Oijen, "Large eddy simulation of the cambridge/sandia stratified flame with flamelet-generated manifolds: Effects of non-unity lewis numbers and stretch," *Combustion and Flame*, vol. 227, 2021.

[23] M. S. Sweeney, S. Hochgreb, M. J. Dunn, and R. S. Barlow, "The structure of turbulent stratified and premixed methane/air flames ii: Swirling flows," *Combustion and Flame*, vol. 159, no. 9, 2012.

[24] R. Zhou, S. Balusamy, M. S. Sweeney, R. S. Barlow, and S. Hochgreb, "Flow field measurements of a series of turbulent premixed and stratified methane/air flames," *Combustion and Flame*, vol. 160, no. 10, 2013.

[25] M. Euler, R. Zhou, S. Hochgreb, and A. Dreizler, "Temperature measurements of the bluff body surface of a swirl burner using phosphor thermometry," *Combustion and Flame*, vol. 161, no. 11, 2014.

[26] B. E. Launder, G. J. Reece, and W. Rodi, "Progress in the development of a reynolds-stress turbulent closure.," *Journal of Fluid Mechanics*, vol. 68, no. 3, pp. 537–566, 1975.

[27] R. Lindstedt and E. Vaos, "Transported pdf modeling of high-reynolds-number premixed turbulent flame," *Combustion and Flame*, vol. 145, 2006.

[28] M. Kuron, Z. Ren, E. R. Hawkes, H. Zhou, H. Kolla, J. H. Chen, and T. Lu, "A mixing timescale model for tpdf simulations of turbulent premixed flames," *Combustion and Flame*, vol. 177, 2017.

[29] "Ansys fluent udf manual," 2011.

[30] Wikipedia contributors, *Turbulence modeling — Wikipedia, the free encyclopedia*, [Online; accessed 7-June-2021], 2021. [Online]. Available:
.

[31] "Ansys fluent theory guide 12.0," vol. 12, 2009.

[32] J. W. K. Janicka and W. Kollmann, "Closure of the transport equation for the probability density function of turbulent scalar fields.," *Non Equilibrium Thermodynamics*, vol. 4, 1977.

[33] C. Dopazo and E. E. O'Brien, "Functional formulation of nonisothermal turbulent reactive flows," *The Physics of Fluids*, vol. 17, no. 11, pp. 1968–1975, 1974.

[34] R. Borghi and T. Mantel, "A new model of premixed wrinkled flame propagation based on a scalar dissipation equation," *Combustion and Flame*, vol. 96, 1994.

[35] T. Kuan, R. Lindstedt, and E. Vaos, "Advances in confined detonations and pulse detonation engines," *Torus Press*, 2003.

[36] O. Chatakonda, E. R. Hawkes, A. J. Aspden, A. R. Kerstein, H. Kolla, and J. H. Chen, "On the fractal characteristics of low damköhler number flames," *Combustion and Flame*, vol. 160, 2013.

[37] T. Lu and C. Law, "A criterion based on computational singular perturbation for the identification of quasi steady state species: A reduced mechanism for methane oxidation with no chemistry," *Combustion and Flame*, vol. 154, 2008.